Semiclassical treatment of the vibrational spectroscopy of OCS

Eric E. Aubanel and David M. Wardlaw

Citation: The Journal of Chemical Physics **88**, 495 (1988); doi: 10.1063/1.454177
View online: http://dx.doi.org/10.1063/1.454177
View Table of Contents: http://scitation.aip.org/content/aip/journal/jcp/88/2?ver=pdfcov
Published by the AIP Publishing

Semiclassical treatment of the vibrational spectroscopy of OCS

Eric E. Aubanel[a] and David M. Wardlaw[b]
Department of Chemistry, Queen's University Kingston, Ontario, K7L 3N6, Canada

(Received 28 July 1987; accepted 16 September 1987)

The utility of a primitive semiclassical method for the quantitative prediction of vibrational eigenvalues and electric dipole transition intensities in triatomic molecules is assessed for the particular case of rotationless OCS in its ground electronic state by comparison to exact quantum calculations. The semiclassical method is based on numerical integration of appropriately selected classical trajectories. The potential energy function determined by Foord, Smith, and Whiffen [Mol. Phys. **29**, 1685 (1975)] and the electric dipole moment function determined by Tanaka, Tanaka, and Suzuki [J. Chem. Phys. **82**, 2835 (1985)] provide the model of the OCS system. Eigenvalues are obtained by the method of adiabatic switching, the number of trajectories required for this purpose being minimized to four using an extension of Johnson's Fourier series method [J. Chem. Phys. **83**, 1204 (1985)]. The resulting semiclassical vibrational transition frequencies (with respect to the ground state) agree with the corresponding quantum frequencies to within 1 cm^{-1} (2 cm^{-1}) for 112 (128) of the 145 converged quantum levels, with the largest discrepancy being 5.2 cm^{-1}. The semiclassical frequencies are compared to the experimental results of Fayt [Ann. Soc. Sci. Brux. **86**, 61 (1972)] and to the semiclassical results of Colwell [Chem. Phys. **46**, 165 (1980)]. The sets of 176 semiclassical and 145 converged quantum transition frequencies reported here are the most extensive and complete to date, the highest energy level being $\sim$7500 cm^{-1} above the ground state. The methodology of Wardlaw, Noid, and Marcus [J. Phys. Chem. **88**, 536 (1984)] for the determination of semiclassical transition intensities in 2*D* oscillator systems is herein extended to the vibrational degrees of freedom in triatomic molecules. For numerous transitions from the ground state and from several low-lying excited states, the semiclassical intensities agree with the quantum intensities to within 6% in the absence of resonances in the associated approximate eigentrajectories. When resonances are involved, the primitive semiclassical treatment is found to be far less accurate, as is expected. A numerical determination of the classical actions, Fourier spectra of the coordinates, surfaces of section, and 2*D* slices through configuration space are presented for representative resonant and nonresonant approximate eigentrajectories. The inherent uncertainties in the semiclassical energy levels and in the transition intensities (if no resonant trajectories are involved) are found to provide a very reliable upper bound on the difference between the semiclassical and quantum results.

I. INTRODUCTION

The purpose of this paper is twofold. First, it systematically extends and improves the methodology for the (primitive) semiclassical evaluation of vibrational transition intensities to triatomic molecules. Earlier theoretical work in this area is confined to diatomic vibrational motion,[1-3] to a limited preliminary study of rotationless OCS[2], and to models of 2*D* coupled oscillator systems.[4] This study is therefore intended to provide a necessary step in the development of a comprehensive semiclassical description of the infrared spectroscopy of small polyatomics. The advantages and disadvantages of the semiclassical approach have been discussed elsewhere.[4] Ultimately rotational transitions must be included, but no attempt is made to do so here; we merely point out that the necessary groundwork is now being laid for the semiclassical treatment of molecular rotations. For example, methods for obtaining the semiclassical rovibrational eigenvalues of simplified models of several triatomics have recently been developed and applied,[5] and Adams[6] has obtained semiclassical spectra for a rotating diatomic using the methodology of Ref. 4. Second, it serves to assess the feasibility and utility of incorporating the recently developed adiabatic switching method (ASM)[7,8] in our semiclassical spectral method. The ASM, in comparison to other trajectory-based semiclassical methods, offers the possibility of considerable computational savings in obtaining the appropriate classical eigentrajectories with which to determine the semiclassical transition intensities. The ASM also provides, with minimum computational effort, semiclassical eigenvalues and it is of equal interest to assess their accuracy.

The list of triatomics for which semiclassical vibrational eigenvalues have been obtained has grown slowly over approximately the last 10 years and includes OCS,[9,10] SO_2,[11,12] H_2O,[11,12] H_3^+,[12,13] D_3^+,[13] T_3^+,[13] and CO_2.[12] Our selection of the OCS molecule was motivated by the following considerations:

(i) A potential energy function[14] and a dipole moment function[15] are available; both are derived by inversion of measured infrared data.

[a] NSERC of Canada Postgraduate Fellow.
[b] NSERC of Canada University Research Fellow.

 0021-9606/88/020495-23$02.10

(ii) Semiclassical eigenvalues of OCS have been obtained by other workers[9,10] using methods other than adiabatic switching. It will therefore be possible to assess the relative accuracy of the ASM for this system.

(iii) An extensive experimental set of OCS vibrational levels has been reported by Fayt.[16] There are no existing theoretical predictions for some of the upper energy levels of this set, primarily because the semiclassical methods which have been applied previously tend not to converge as the OCS vibrational energy increases. It is conceivable that the ASM will not fail in an analogous manner, offering the possibility of assessment of the accuracy of the potential energy function at energies above the highest vibrational levels employed in the original potential energy fitting procedure.[14]

(iv) Dynamically tuned resonances, especially the 4:1 Fermi resonance between the low-frequency bend and the high-frequency asymmetric stretch, are known to play a role in the spectroscopy[16] and classical dynamics[17] of OCS. Since nonlinear resonances are expected to be commonplace in polyatomic molecules, it becomes important to assess the extent and nature of the breakdown of a primitive semiclassical treatment of the vibrational spectroscopy in such a case.

(v) The linear equilibrium geometry of OCS means that there are four vibrational degrees of freedom. Two of these constitute a doubly degenerate bend and the other two are singly degenerate stretching modes. Approximate semiclassical correspondence rules, which are presented later, have been examined for models of isolated $2D$ bending[4] and $1D$ stretching[3] vibrations. The case at hand allows us to test these rules in the presence of a "bath" of coupled degrees of freedom, introducing improvements as necessary.

Rather than include a review of the development of the many and varied semiclassical methods, we refer the reader to several recent papers. A concise yet thorough summary of existing approaches to the semiclassical quantization problem is found in Sec. I of Ref. 18. The historical development and theory of the semiclassical treatment of vibrational intensities is summarized in Sec. III of Ref. 4; several complementary studies[19,20] have since been published. Reference 31 provides a recent review of applications of the semiclassical spectral method.

The paper is organized as follows: Section II gives the Hamiltonian and electric dipole moment functions used to model the OCS molecule. The semiclassical theory for the eigenvalues, transition intensities, and dipole moment averages, as it pertains to OCS, is described in Sec. III along with the various methods used later to assess the approximate eigentrajectories generated by the ASM. The quantum calculation is outlined in Sec. IV. Results for eigenvalues, transition intensities, and dipole averages are presented and discussed in Sec. V. Also included in Sec. V, for a few resonant and nonresonant approximate eigentrajectories, are a numerical determination of the actions, typical coordinate spectra, and pictorial representations of the phase space structure. A summary is provided in Sec. VI.

II. MODEL OF OCS

A. Hamiltonian

The Hamiltonian H given below is that used in three previous studies[9,10,14] of the vibrational eigenvalues of OCS. It is obtained from Watson's[21] expression for Hougen's[22] so-called isomorphic rotation–vibration Hamiltonian for a linear triatomic by setting the overall rotational angular momentum to zero. Here it is convenient to write H as the sum of a separable zeroth-order Hamiltonian H_0 and a nonseparable interaction term H_I:

$$H = H_0 + H_I. \tag{2.1}$$

H_0 describes the motion of the four uncoupled normal vibrational modes of OCS—the two nondegenerate stretching modes (designated 1 for the symmetric stretch and 3 for the asymmetric stretch) and the doubly degenerate bend (designated 2). It is expressed as a sum of three Hamiltonians, one for each type of motion

$$H_0 = \sum_{i=1}^{3} H_{i,0}. \tag{2.2}$$

The four normal coordinates are q_1, $\mathbf{q}_2 = (q_{2x}, q_{2y})$, and q_3 and their respective conjugate momenta p_1, $\mathbf{p}_2 = (p_{2x}, p_{2y})$, and p_3. The $2D$ vector $\mathbf{q}_2$ describes the bending displacement in the x–y plane, which is perpendicular to a z axis which is aligned with the molecular axis in the equilibrium configuration. In terms of these variables and the unperturbed frequencies $\omega_{i,0}$, the $H_{i,0}$'s are

$$H_{k,0} = \tfrac{1}{2}(p_k^2 + \omega_{k,0}^2 q_k^2), \quad k = 1,3, \tag{2.3}$$

$$H_{2,0} = \tfrac{1}{2}(\mathbf{p}_2\cdot\mathbf{p}_2 + \omega_{2,0}^2 \mathbf{q}_2\cdot\mathbf{q}_2)$$
$$= \tfrac{1}{2}[p_{2x}^2 + p_{2y}^2 + \omega_{2,0}^2 (q_{2x}^2 + q_{2y}^2)]. \tag{2.4}$$

For subsequent simplification, it is expedient to introduce polar coordinates for mode 2. The new coordinates are the radius $q_2 = |\mathbf{q}_2|$ and the angle $\alpha_l = \tan^{-1}(q_{2y}/q_{2x})$; the corresponding conjugate momenta are the radial momentum $p_{2r} = \mathbf{p}_2\cdot\mathbf{q}_2/|\mathbf{q}_2|$ and the z component $L_z = \mathscr{L} = |\mathbf{q}_2\times\mathbf{p}_2|$ of the vibrational angular momentum $\mathbf{L}$. In terms of these new variables, Eq. (2.4) becomes

$$H_{2,0} = \tfrac{1}{2}(p_{2r}^2 + \mathscr{L}^2/q_2^2 + \omega_{2,0}^2 q_2^2). \tag{2.5}$$

The interaction term is a sum of a vibrational kinetic energy term T_v and a potential energy function V:

$$H_I = T_v + V. \tag{2.6}$$

The T_v contribution is determined by the x and y components of $\mathbf{L}$:

$$T_v = \tfrac{1}{2}\mu\,(L_x^2 + L_y^2) = \tfrac{1}{2}\mu\,[\zeta_{21}(\mathbf{q}_2 p_1 - q_1\mathbf{p}_2)$$
$$+ \zeta_{23}(\mathbf{q}_2 p_3 - q_3\mathbf{p}_2)]^2, \tag{2.7}$$

where $\mu = I^0/(I^0 + a_1 q_1/2 + a_3 q_3/2)^2$, I^0 is the moment of inertia for OCS in its linear equilibrium configuration, $\zeta_{21}(=-\zeta_{12})$ and ζ_{23} are Coriolis coupling coefficients, $a_1 = 2\zeta_{23}(I^0)^{1/2}$, and $a_3 = 2\zeta_{21}(I^0)^{1/2}$. The potential energy function employed is that determined by Foord, Smith, and Whiffen (FSW)[14] on the basis of a best fit of calculated to observed spectral quantities. It is a 16 parameter polymonial in q_1, q_2, and q_3 and includes all nonzero cubic and quartic terms plus one quintic term

$$V = \sum_{i,j,k}{}' k_{ijk} q_i q_j q_k + \sum_{i,j,k,l}{}' k_{ijkl} q_i q_j q_k q_l + k_{22223} q_2^4 q_3, \tag{2.8}$$

where the primes indicate that the summations are restricted by $i \leqslant j \leqslant k \leqslant l$.

TABLE I. Parameters for the $^{16}O^{12}C^{32}S$ Hamiltonian.

Constant[a]	Value
ω_1 (cm^{-1})	875.70
ω_2 (cm^{-1})	523.62
ω_3 (cm^{-1})	2092.46
$k_{111}/\omega_1^{3/2}$ (cm^{-1})	− 33.59
$k_{113}/\omega_1\omega_3^{1/2}$ (cm^{-1})	53.52
$k_{122}/\omega_1^{1/2}\omega_2$ (cm^{-1})	42.95
$k_{133}/\omega_1^{1/2}\omega_3$ (cm^{-1})	− 125.24
$k_{223}/\omega_2\omega_3^{1/2}$ (cm^{-1})	51.30
$k_{333}/\omega_3^{3/2}$ (cm^{-1})	− 67.01
k_{1111}/ω_1^2 (cm^{-1})	1.55
$k_{1113}/\omega_1^{3/2}\omega_3^{1/2}$ (cm^{-1})	− 4.40
$k_{1122}/\omega_1\omega_2$ (cm^{-1})	− 4.95
$k_{1133}/\omega_1\omega_3$ (cm^{-1})	6.40
$k_{1223}/\omega_1^{1/2}\omega_2\omega_3^{1/2}$ (cm^{-1})	− 2.38
$k_{1333}/\omega_1^{1/2}\omega_3^{3/2}$ (cm^{-1})	0.84
k_{2222}/ω_2^2 (cm^{-1})	1.77
$k_{2233}/\omega_2\omega_3$ (cm^{-1})	− 19.28
k_{3333}/ω_3^2 (cm^{-1})	3.98
$k_{22223}/\omega_2^2\omega_3^{1/2}$ (cm^{-1})	− 0.45
I^0 (uÅ^2)	82.96
a_1($u^{1/2}$Å)	17.90
a_3($u^{1/2}$Å)	3.31
ζ_{12}	− 0.1815
ζ_{23}	0.9833

[a] ω_i in the table corresponds to $\omega_{i,0}$ in the text ($i = 1,2,3$).

The potential parameters appearing in the expressions for H_0, T_v, and V are listed in Table I. Note that V is an even function of q_2 and that T_v is independent of α_l. That the latter is true classically can be seen by expanding the last equality of Eq. (2.7) and assuming that q_i and p_i commute ($i = 1,2x,2y,3$):

$$T_v^{cl} = \frac{\mu}{2}\{\zeta_{21}^2\,[p_1^2q_2^2 + q_1^2p_2^2 - 2p_1q_1(\mathbf{p}_2\cdot\mathbf{q}_2)] + \zeta_{23}^2\,[p_3^2q_2^2 + q_3^2p_2^2 - 2p_3q_3(\mathbf{p}_2\cdot\mathbf{q}_2)] + 2\zeta_{21}\zeta_{23} \times [p_1p_3q_2^2 + q_1q_3p_2^2 - (q_1p_3 + p_1q_3)(\mathbf{p}_2\cdot\mathbf{q}_2)]\}, \tag{2.9}$$

where $p_2^2 = |\mathbf{p}_2|^2 = p_{2r}^2 + \mathcal{L}^2/q_2^2$, $q_2^2 = |\mathbf{q}_2|^2$, and $\mathbf{p}_2\cdot\mathbf{q}_2 = p_{2r}q_2$. The Hamiltonian H is therefore independent of α_l and so $\mathcal{L}$ is a constant of the motion, a feature which significantly reduces the computational effort involved in the ensuing semiclassical and quantum calculations. The quantum treatment of T_v [Eq. (2.7)] is discussed in Sec. IV.

B. Dipole moment function

Intensities for transitions between states and expectation values of the dipole moment in a given state were calculated, both semiclassically and quantum mechanically, using a representation of the electric dipole moment function recently obtained by Tanaka, Tanaka, and Suzuki.[15] These authors used a least-squares analysis to fit measured dipole moments and transition intensities to the corresponding quantities calculated by matrix diagonalization of the Hamiltonian described in Sec. II A. The form of the dipole function most convenient for our purposes are the expansions, in dimensionless normal coordinates [$Q_i = (\omega_{i,0}/\hbar)^{1/2}q_i$, $i = 1,2,3$] of the Cartesian components of the dipole vector $\boldsymbol{\mu}$:

$$\mu_z = \mu_e + \mu_z^1Q_1 + \mu_z^3Q_3 + \mu_z^{11}Q_1^2/2 + \mu_z^{13}Q_1Q_3 + \mu_z^{33}Q_3^2/2 + \mu_z^{22}Q_2^2/2 + \mu_z^{111}Q_1^3/6 + \mu_z^{113}Q_1^2Q_3/2 + \mu_z^{133}Q_1Q_3^2/2 + \mu_z^{333}Q_3^3/6 + \mu_z^{122}Q_1Q_2^2/2 + \mu_z^{223}Q_2^2Q_3/2, \tag{2.10}$$

$$\mu_x = \mu_x^2Q_{2x}, \tag{2.11}$$

where μ_e is the equilibrium dipole moment and the coefficients are the derivatives of μ_z or μ_x with respect to the normal coordinates and evaluated at equilibrium, e.g., $\mu_z^1 = (\partial\mu_z/\partial Q_1)_e$, $\mu_z^{33} = (\partial^2\mu_z/\partial Q_3^2)_e$, $\mu_z^{223} = (\partial^3\mu_z/\partial^2Q_{2x}^2\partial Q_3)_e$, $\mu_x^2 = (\partial\mu_x/\partial Q_{2x})_e$. The numerical values of the coefficients in Eqs. (2.10) and (2.11) are listed in Table II. The y component of μ is obtained by replacing Q_{2x} by Q_{2y} in Eq. (2.11) and noting that the expansion coefficients for μ_x and μ_y are identical by symmetry. For this reason, transition intensities and dipole moment expectation values determined only by μ_x and μ_z need be considered.

III. SEMICLASSICAL TREATMENT

Since the method used to obtain the transition frequencies is different from that used for the transition intensities, these two topics are discussed separately in Secs. III A and III B. The identification and analysis of nonlinear resonances in the OCS system is the subject of Sec. III C.

A. Transition frequencies

Frequencies of transitions between pairs of vibrational states are obtained as semiclassical eigenvalue differences; the vibrational eigenvalues are determined via the ASM as follows: a time-dependent Hamiltonian, based on Eq. (2,1), is first defined

$$H(t) = H_0 + \lambda(t)H_I, \tag{3.1}$$

where $\lambda(t)$ is an adiabatic switching function, chosen so as to vary slowly from $\lambda(0) = 0$ to $\lambda(T) = 1$. Classical initial

TABLE II. Dipole moment derivatives for $^{16}O^{12}C^{32}S$ with respect to dimensionless normal coordinates.[a]

Derivative	Value (D)
μ_e	0.714 70
$(\partial\mu_z/\partial Q_1)_e$	− 0.091 59
$(\partial\mu_z/\partial Q_3)_e$	0.552 7
$(\partial\mu_x/\partial Q_{2x})_e$	− 0.068 26
$(\partial^2\mu_z/\partial Q_1^2)_e$	0.008 30
$(\partial^2\mu_z/\partial Q_1\partial Q_3)_e$	0.007 08
$(\partial^2\mu_z/\partial Q_3^2)_e$	− 0.015 57
$(\partial^2\mu_z/\partial Q_{2x}^2)_e$	− 0.004 402
$(\partial^3\mu_z/\partial Q_1^3)_e$	− 0.001 583
$(\partial^3\mu_z/\partial Q_1^2\partial Q_3)_e$	0.000 823
$(\partial^3\mu_z/\partial Q_1\partial Q_3^2)_e$	− 0.002 088
$(\partial^3\mu_z/\partial Q_3^3)_e$	− 0.004 504
$(\partial^3\mu_z/\partial Q_1\partial Q_{2x}^2)_e$	− 0.000 272
$(\partial^3\mu_z/\partial Q_{2x}^2\partial Q_3)_e$	− 0.009 39

[a] Taken from case I of Ref. 15.

conditions (discussed below) corresponding to a particular semiclassical vibrational state of OCS are readily determined from H_0 since it is separable. Hamilton's equations of motion for $H(t)$ are then integrated numerically from $t=0$ to $t=T$. If the adiabatic hypothesis holds, the classical actions will be conserved and the quantizing initial conditions imposed on H_0 will be valid for $H(T)=H$. The semiclassical eigenvalue is then trivially obtained by evaluating the energy of the trajectory at $t=T$.

The s_2 switching function introduced by Johnson[8] and used extensively elsewhere,[7,13,23]

$$\lambda(t)=t/T-[\sin(2\pi t/T)/2\pi], \tag{3.2}$$

was employed in the determination of all semiclassical results reported in Sec. V. Preliminary calculations employing Johnson's s_4 switching function,[8] which he found to be superior to s_2 for the linearly forced oscillator, revealed no such advantage for the system studied here. Selection of an optimal switching time T' is discussed later.

We now consider the problem of finding initial conditions for H_0, beginning with modes 1 and 3. The classical action and zeroth order energy for a harmonic oscillator are

$$\begin{aligned} I_i &= (n_i+\tfrac{1}{2})\hbar, \\ E_{i,0} &= I_i\omega_{i,0}, \end{aligned} \qquad i=1,3, \tag{3.3}$$

where n_i is the vibrational quantum number for mode i. The initial coordinates and momenta are

$$q_{i,0}=\left[\frac{2E_{i,0}}{\omega_{i,0}^2}\right]^{1/2}\sin(\alpha_i-\frac{\pi}{2}), \tag{3.4a}$$

$$i=1,3; \quad 0\leqslant\alpha_i\leqslant\pi$$

$$p_{i,0}=\pm\left[2E_{i,0}-\omega_{i,0}^2q_{i,0}^2\right]^{1/2}, \tag{3.4b}$$

where α_i is the angle conjugate to I_i.

The classical actions and zeroth order energy for mode 2 are

$$\begin{aligned} &I_{2r}=(n_{2r}+1/2)\hbar; \quad \mathscr{L}=l\hbar, \\ &I_2=(n_2+1)\hbar, \quad E_{2,0}=I_2\omega_{2,0} \end{aligned} \tag{3.5}$$

where $n_2=2n_{2r}+l$ is the principal quantum number, n_{2r} is the radial quantum number, l is the angular momentum quantum number associated with the classical angular momentum action $\mathscr{L}$, and, for a given positive value[24] of l, the possible values of n_2 are seen to be l, $l+2$, $l+4$,... . The unperturbed classical motion of a doubly degenerate bend has been considered in detail by Noid and Marcus[25] in their study of the Hénon–Heiles system whose zeroth-order Hamiltonian is equivalent to $H_{2,0}$. They point out that there are two classes of trajectories—precessing and librating, corresponding to $\mathscr{L}\neq 0$ and $\mathscr{L}=0$, respectively. It is expedient to consider the two cases separately.

1. $\mathscr{L}\neq 0$

The unperturbed motion is an elliptical periodic trajectory centered on the origin and the complete family of such trajectories is generated by rotating this ellipse about the origin. The time dependence of the motion is given by Hamilton's equations for the angles α_2 and α_l conjugate to I_{2r} and $\mathscr{L}$, respectively: $\dot{\alpha}_2=\partial H_{2,0}/\partial I_{2r}=2\omega_{2,0}$ and $\dot{\alpha}_l=\partial H_{2,0}/\partial\mathscr{L}=\omega_{2,0}$. The value of $\alpha_l(t)$ at $t=0$, denoted α_l, simply selects one ellipse from the family of ellipses and can therefore be ignored. (Alternatively, α_l can be interpreted as specifying the orientation of an x–y coordinate system relative to some space-fixed system and this clearly will not affect the physics.) The value of $\alpha_2(t)$ at $t=0$, denoted α_2, determines the initial radial coordinate $q_{2,0}$ and the initial radial momentum $p_{2r,0}$, which together specify the starting position on the ellipse

$$q_{2,0}=\frac{1}{\omega_{2,0}}\left[(E_{2,0}^2-\mathscr{L}^2\omega_{2,0}^2)^{1/2}\times\sin(\alpha_2-\frac{\pi}{2})+E_{2,0}\right]^{1/2}, \quad 0\leqslant\alpha_2\leqslant\pi \tag{3.6a}$$

$$p_{2r,0}=\pm\left[2E_{2,0}-\frac{\mathscr{L}^2}{q_{2,0}^2}-\omega_{2,0}^2q_{2,0}^2\right]^{1/2}. \tag{3.6b}$$

The derivation of Eq. (3.6) is outlined in Appendix A.

2. $\mathscr{L}=0$

In this case there is no centrifugal repulsion and the periodic trajectory along each ellipse degenerates into an oscillation along a straight line passing through the origin. Noid and Marcus demonstrate that the semiclassical quantization conditions remain $I_{2r}=(n_{2r}+1/2)\hbar$ and $I_2=(2n_{2r}+0+1)\hbar=(n_2+1)\hbar$. The motion is just a 1D harmonic oscillation and so the initial conditions $q_{2,0}$ and $p_{2,0}$ are provided by Eq. (3.4) with $i=2$ and $E_{2,0}=(n_2+1)\hbar$. Note that $p_{2r}=\mathbf{p}\cdot\mathbf{q}/|\mathbf{q}|$ reduces to p_2 for $l=0$. The classical picture, which puts all the zero-point energy of $1\hbar$ in the 1D vibration, is at odds with the purely quantum picture which maintains zero-point energy of $\hbar/2$ in each of the x and y degrees of freedom. This is known to lead to small errors in the primitive semiclassical eigenvalues of $l=0$ states in the Hénon–Heiles system.[7,25,30] Further comments on the classical treatment of mode 2 for $l=0$ are made in Sec. V.

For all three modes values of α_i on the range $(\pi,2\pi)$ are achieved by choosing the negative sign for the momenta in Eqs. (3.4b) and (3.6b).

According to the adiabatic hypothesis,[26] the final eigenvalue E is determined only by the quantized action $\mathbf{I}=(I_1,I_2,I_3)$ and is independent of $\boldsymbol{\alpha}=(\alpha_1,\alpha_2,\alpha_3)$. This is true, in principle, for an infinitely large switching interval $T\to\infty$. In practice, however, T must be finite and E becomes a function of $\mathbf{I}$, $\boldsymbol{\alpha}$, and T. An approximation to $E(\mathbf{I})$ is obtained by averaging $E(\mathbf{I},\boldsymbol{\alpha},T)$ over an ensemble of $\boldsymbol{\alpha}$'s for a given value of T, monitoring the dependence of $\overline{E}(\mathbf{I},T)$ on T, and making the assignment $E(\mathbf{I})\simeq\overline{E}(\mathbf{I},T')$, where T' is the value of T at which $\overline{E}(\mathbf{I},T)$ is deemed to have converged. A common measure of this convergence,[7,8] and that used here, is the rms deviation $\Delta E_{\rm rms}(\mathbf{I},T)$ from the mean $\overline{E}(\mathbf{I},T)$.

There are several possibilites for generating an ensemble of trajectories suited to the approximate implementation of the adiabatic hypothesis. One approach is to select the angle variables $\boldsymbol{\alpha}$ at random. In an earlier numerical study,[7] it was found that ~ 25 trajectories were required to obtain sufficiently converged eigenvalues in reasonably short switching

times ($\sim$70 characteristic vibrational periods for the systems studied there); this was also found to be the case in our study as is discussed below. Naturally, one would like to minimize the number of trajectories needed to obtain an energy level, while also maintaining T' at a minimum. This is especially important here since the semiclassical intensity calculations described in Sec. III B require relatively long trajectory times to achieve convergence. To this end, we have extended to three dimensions the Fourier analysis technique developed by Johnson[8] for two dimensions; the general treatment is given in Appendix B 1. Application of this technique, as described in Appendix B 2, to a small number of selected vibrational states indicated that an excellent approximation to the mean eigenvalue is provided by averaging the energies of four particular trajectories

$$\bar{E} = \{E[\mathbf{I},T,\alpha = (0,0,0)] + E[\mathbf{I},T,\alpha = (0,\pi/2,\pi/2] + E[\mathbf{I},T,\alpha = (0,\pi,\pi)] + E[\mathbf{I},T,\alpha = (0,3\pi/2,3\pi/2)\}/4. \quad (3.7)$$

This expression was then assumed to be valid for all I and used to provide all semiclassical eigenvalues and approximate eigentrajectories required in this study. The rms deviation $\Delta E_{\rm rms}$ of the four energies in Eq. (3.7) from $\bar{E}$ is used to provide some measure of the uncertainty in $\bar{E}$.

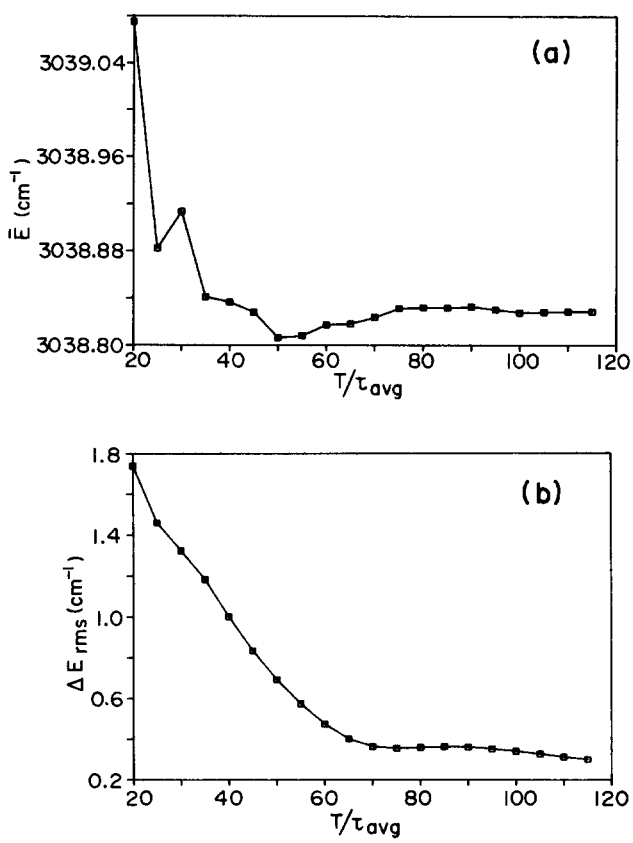

FIG. 1. Plots of (a) the average energy $\bar{E}$ of the group of four trajectories and (b) the associated rms deviation $\Delta E_{\rm rms}$ vs the switching time T for the state (0 2^2 0). Note that the abscissa is the unitless quantity $T/\tau_{\rm avg}$, where $\tau_{\rm avg} = (\tau_1 + \tau_2 + \tau_3)/3$ is an average OCS vibrational period and that the scale begins at 20.

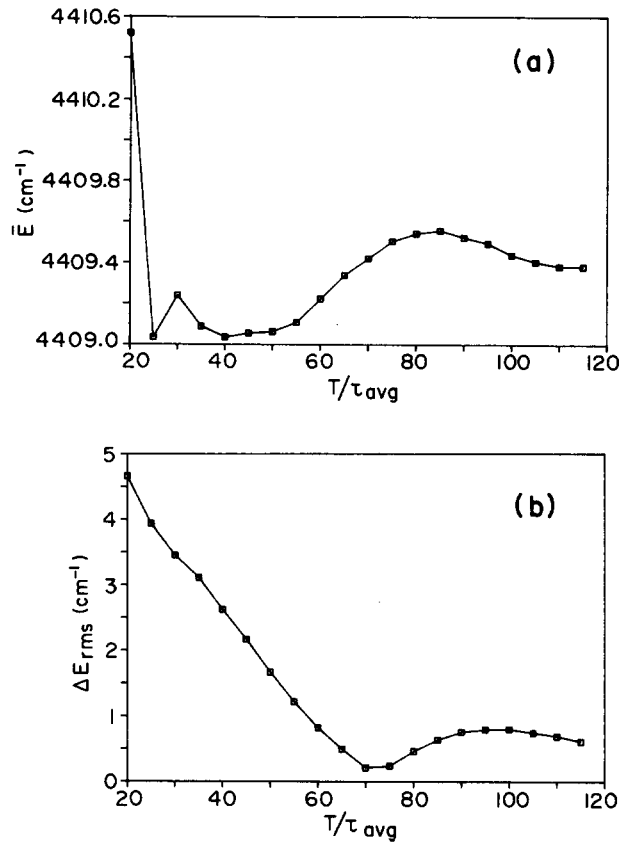

FIG. 2. The same as Fig. 1, but for the state (1 3^1 0).

To determine the optimum switching time, plots of $\bar{E}$ vs T and $\Delta E_{\rm rms}$ vs T were examined for selected vibrational states. Figures 1, 2 and 3 display such plots for the states $(n_2 n_2^l n_3) = (0\,2^2\,0)$, $(1\,3^1\,0)$, and $(0\,4^0\,2)$, respectively, and reflect the observed diversity in the dependence of $\bar{E}$ and $\Delta E_{\rm rms}$ on T. The abscissa in these figures is the dimensionless quantity $T/\tau_{\rm avg}$, where the average OCS vibrational period is defined to be $\tau_{\rm avg} = (\tau_1 + \tau_2 + \tau_3)/3$ and $\tau_i = 2\pi/\omega_{i,0}$. In Figs. 1 and 2, it can be seen that $\bar{E}$ (upper panels) has stabilized to within $\Delta E_{\rm rms}$ (lower panels) for $T > \sim 70\tau_{\rm avg}$, a feature shared by most other states analyzed in this manner. This motivated the choice $T' = 70\tau_{\rm avg}$ as the optimum (i.e., minimum) switching time for our system. Figure 3 is noteworthy in that $\bar{E}$ steadily decreases with increasing T and $\Delta E_{\rm rms}$ is comparatively large and increases with increasing T. Of all states whose $\bar{E}$ and $\Delta E_{\rm rms}$ values were examined as a function of T, (0 4^0 2) was the only one found to display such behavior, presumably because some or all of the four trajectories are being switched through a sufficiently large region of resonant or chaotic phase space.

B. Transition Intensities

For both quasiperiodic and ergodic motion, it has been shown[27] that the classical power spectrum $I_f(\omega)$ is related to the Fourier transform of the classical dynamical variable $f(t)$:

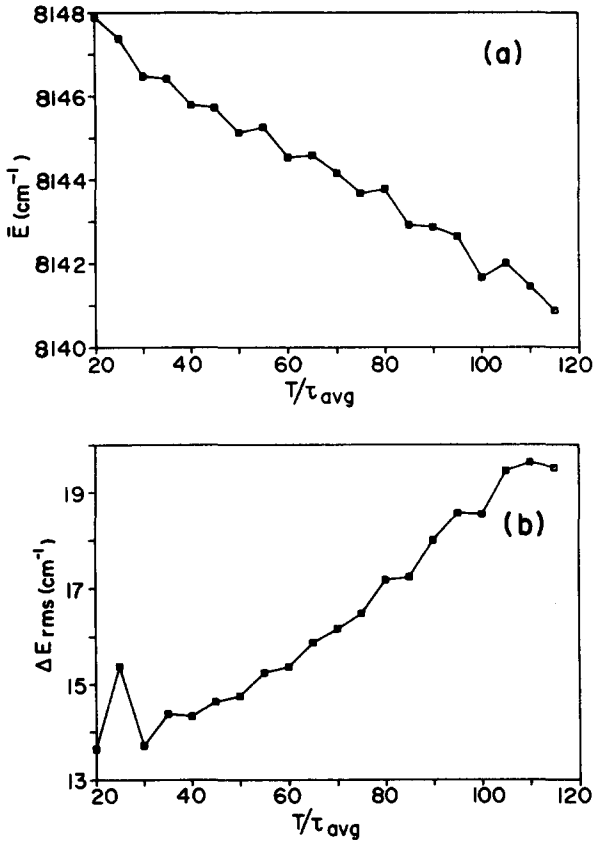

FIG. 3. The same as Fig. 1, but for the state (0 4⁰ 2).

$$I_f(\omega) = \frac{1}{2\pi} \lim_{T\to\infty} \frac{1}{T} \left| \int_0^T dt f(t) \exp(-i\omega t) \right|^2, \quad (3.8)$$

where the time dependence of f is obtained by integrating, in the case of a nondegenerate system, a single trajectory[28] for total time T. For a transition the connection between quantum and classical spectra is clear, at present, only for classically regular or quasiperiodic motion to which our study is restricted. For the electric dipole transitions considered here, f is taken to be μ_z or μ_x [Eqs. (2.10) and (2.11)]. Details of the determination of the Fourier transform of $\mu_\beta(t)$ ($\beta = z$ or x) are given in Appendix C. We note that the determination of $\mu_x(t)$ from a trajectory requires special consideration. Since all trajectories used in the calculation of μ_x transition intensities have $l \neq 0$, the radial coordinate $q_2 = (q_{2x}^2 + q_{2y}^2)^{1/2}$, and not q_{2x}, is the variable of integration in Hamilton's equations. The time series for $q_{2x} \sim \mu_x$ is $q_{2x}(t) = q_2(t)\cos\alpha_l(t)$, where $\alpha_l(t)$ is obtained by integrating the additional equation $\dot{\alpha}_l = \partial H/\partial \mathscr{L}$ with $\alpha_l(0) = 0$.

The idea of spectral intensities being related to Fourier coefficients is an old one, dating back to the era of old quantum theory.[29] The derivation of such a relation for a general multidimensional system has been given by Wardlaw, Noid, and Marcus (WNM)[4] and is reproduced here to emphasize several important assumptions. Consider the semiclassical matrix element of a dipole operator μ for the transition from some initial state $|\mathbf{m}\rangle$ with action $\mathbf{J}(\mathbf{m})$ to a final state $|\mathbf{m}'\rangle$ with actions $\mathbf{J}'(\mathbf{m}')$ and assume that all classical motion is quasiperiodic:

$$\begin{aligned}
\langle \mathbf{m}'|\mu|\mathbf{m}\rangle &= \int_0^{2\pi} \langle \mathbf{m}'|\boldsymbol{\theta}\rangle\langle\boldsymbol{\theta}|\mu|\mathbf{m}\rangle d\boldsymbol{\theta} \\
&\approx \int_0^{2\pi} \langle \mathbf{m}'|\boldsymbol{\theta}\rangle \mu(\mathbf{J}^c,\boldsymbol{\theta})\langle\boldsymbol{\theta}|\mathbf{m}\rangle d\boldsymbol{\theta} \\
&\approx \int_0^{2\pi} e^{-i\mathbf{m}'\cdot\boldsymbol{\theta}} \sum_{\mathbf{k}} \mu_{\mathbf{k}}(\mathbf{J}^c) e^{i\mathbf{k}\cdot\boldsymbol{\theta}} e^{i\mathbf{m}\cdot\boldsymbol{\theta}} d\boldsymbol{\theta} \\
&= \int_0^{2\pi} \sum_{\mathbf{k}} \mu_{\mathbf{k}}(\mathbf{J}^c) e^{i\mathbf{k}\cdot\boldsymbol{\theta}} e^{-i\boldsymbol{\Delta}\cdot\boldsymbol{\theta}} d\boldsymbol{\theta} \\
&= \sum_{\mathbf{k}} \mu_{\mathbf{k}}(\mathbf{J}^c)\delta_{\mathbf{k},\boldsymbol{\Delta}} \\
&= \mu_{\boldsymbol{\Delta}}(\mathbf{J}^c). \qquad (3.9)
\end{aligned}$$

Here $\langle \mathbf{m}|\boldsymbol{\theta}\rangle = \exp(-i\mathbf{m}\cdot\boldsymbol{\theta})$ is the primitive semiclassical wave function, $\boldsymbol{\theta}$ are the angle variables conjugate to $\mathbf{J}$, $\mathbf{J}'$, and $\mathbf{J}^c$, and $\boldsymbol{\Delta} = \mathbf{m}' - \mathbf{m}$. The crucial step in Eq. (3.9), and the one for which there is no known rigorous justification, lies in the second line since it expresses the evaluation of the matrix element in terms of a *single* trajectory with so-called correspondence actions $\mathbf{J}^c = \mathbf{J}^c(\mathbf{m}^c)$. The specification of rules for the correspondence quantum numbers $\mathbf{m}^c$ is consequently approximate, a point to which we return shortly. Writing μ as a Fourier expansion (in the angle variables with coefficients depending only on the actions) in the third line of Eq. (3.9) assumes that the motion is quasiperiodic. In practice, $\mu_{\boldsymbol{\Delta}}$ is obtained via Eq. (3.8) by integrating a quasiperiodic trajectory for a time sufficiently long to ensure uniform coverage of the torus.

Implicit in Eq. (3.9) is the use of the *same* angle variables $\boldsymbol{\theta}$ for both the initial, final, and correspondence states, which tacitly assumes that all three wave functions correspond, classically, to trajectories moving on topologically equivalent tori. This semiclassical approach is therefore not expected to describe transitions in which any one of the initial, final, or correspondence states is characterized by a torus different than that characterizing the other two states, as commonly arises in intrinsically and dynamically resonant systems. In addition, Eq. (3.9) is also not expected to be valid for transitions involving initial and/or final states requiring a uniform semiclassical description. A particular approximate treatment involving a sum of primitive semiclassical intensities was nevertheless quite successful in predicting the intensities of some such transitions in the Hénon–Heiles system as studied by WNM.

For OCS, we employ approximate correspondence rules whose validity has been assessed in several earlier numerical studies[3,4,6] on simpler systems. The advantage of the formulation embodied in Eq. (3.9) is that only a *single* trajectory, with actions $\mathbf{I}^c$, is needed to generate the semiclassical equivalent of the transition matrix element.

The general form of the correspondence rule for intensities is $\mathbf{n}^c = g(\mathbf{n},\boldsymbol{\Delta})$ and several possibilities for the functional form of g are presented below. The simplest and seemingly most natural choice, for a single degree of freedom j, is the arithmetic mean

$$n_j^c = n_j + \Delta_j/2, \tag{3.10}$$

where $\Delta_j = n_j' - n_j$. This choice yields a Hermitian dipole operator[30] and, in the limit $\Delta_j/n_j \ll 1$, approximate agreement between quantum and semiclassical intensities.[2,19] Another rule, suitable for a single vibrational mode and expected to be an improvement over Eq. (3.10), is

$$n_j^c = [(n_j + \Delta_j)!/(n_j)!]^{1/\Delta_j} - \tfrac{1}{2}. \tag{3.11}$$

Naccache[1] arrived at this formula by comparing analytical results for classical Fourier coefficients and quantum matrix elements of q and p for the 1D harmonic oscillator. Equation (3.11) reduces to Eq. (3.10) for $\Delta_j = 1$ and predicts that n_j^c is less than the arithmetic mean for $\Delta_j > 2$. WNM have applied Eq. (3.11) to a 2D incommensurate vibrational system and found it to be more accurate than eq. (3.10) for the two dipole functions considered in that study.

Since mode 2 is described by the polar quantum numbers n_2 and l, neither of which corresponds to a single vibrational degree of freedom, Eq. (3.11) is probably inapplicable, motivating the investigation of a correspondence rule suited to mode 2. The two dipole functions μ_z and μ_x give rise to rigorous selection rules $\Delta l = 0$ and $\Delta l = \pm 1$, respectively, and we restrict our discussion to these two cases.

1. $\Delta l = 0$

The n_2 selection rule for mode 2 is $\Delta_2 = n_2' - n_2 =$ even. Comparison of classical Fourier coefficients of q_2^2 and q_2^4 to quantum matrix elements for three values of Δ_2 in Appendix A leads to the following proposal for a correspondence rule for n_2:

$$n_2^c = \begin{cases} 2[(n_2 + \Delta_2/2)!/(n_2/2)!]^{2/\Delta_2} - 1, & \text{if } \Delta_2 > 0 \\ n_2, & \text{if } \Delta_2 = 0, \end{cases} \tag{3.12}$$

which reduces to Eq. (3.10) for $\Delta_2 = 2$.

2. $\Delta l = \pm 1$

The selection rule is $\Delta_2 =$ odd. At present, it is not known if a rule analogous to Eq. (3.12) exists for this case and we therefore resorted to the arithmetic mean [Eq. (3.10)] for both n_2 and l, a choice which can be heuristically justified as follows: All the μ_x transitions reported in Sec. V have the minimal value $\Delta_2 = 1$ because transitions with $\Delta_2 > 1$ have such exceedingly small intensities as to be of no practical importance. Since both Eqs. (3.11) and (3.12) reduce to Eq. (3.10) for the associated minimal values of $\Delta_j = 1$ and $\Delta_2 = 2$, respectively, we anticipate that a rule designed for the $\Delta l \neq 0$ case would also predict arithmetic means for n_2^c and l^c when $\Delta l = \Delta_2 = 1$.

Semiclassical intensities determined via Eqs. (3.10)–(3.12) are compared later. Note that the components of $\mathbf{n}^c$, as given by the above three equations, are in between the corresponding components of $\mathbf{n}$ and $\mathbf{n}'$ and are not restricted to integer values.

In the discussion so far, it has been assumed that only one correspondence trajectory is required to generate a particular transition intensity and, indeed, this would be the case for an eigentrajectory with actions $\mathbf{I}^c$ and integrated for a sufficiently long time to ensure uniform coverage of the torus. Since it is particularly convenient to generate, via the ASM *approximate* eigentrajectories which depend on $\mathbf{I}^c$, $\boldsymbol{\alpha}$, and T', it was decided to approximate the semiclassical intensity as an average of intensities $I(I^c,T',\boldsymbol{\alpha})$ obtained from an ensemble of these approximate eigentrajectories. This is completely analogous to the approach described in Sec. III A for the semiclassical eigenvalues and, again, there are presumably various possibilities for the choice of the ensemble. Although application of the Fourier analysis technique for eigenvalues (Appendix B) to intensities would probably provide a minimal set of optimal zeroth-order initial conditions from which to generate the averaged intensity, this would have involved extensive computation (because the trajectories involved are now of length $\sim 2000\tau_{\text{avg}}$, instead of the $\sim 70\tau_{\text{avg}}$ required for the eigenvalue study) and was not done. Instead, the same four sets of trajectory initial conditions which determined the eigenvalues via Eq. (3.7) were employed to determine an average intensity $\bar{I} = I(\text{AS})$:

$$\begin{aligned} I(\text{AS}) = \{ & I[\mathbf{I}^c, T', \boldsymbol{\alpha} = (0,0,0)] \\ & + I[\mathbf{I}^c, T', \boldsymbol{\alpha} = (0,\pi/2,\pi/2)] \\ & + I[\mathbf{I}^c, T', \boldsymbol{\alpha} = (0,\pi,\pi)] \} \\ & + I[\mathbf{I}^c, T', \boldsymbol{\alpha} = (0,3\pi/2,3\pi/2)] \}/4, \end{aligned} \tag{3.13}$$

where $I(\mathbf{I}^c,T',\boldsymbol{\alpha})$ is an intensity obtained from a trajectory evolving under H [Eq. (2.1)] with initial conditions equal to the final conditions at $t = T'$ of an adiabatically switched trajectory which has evolved under $H(t)$ [Eq. (3.1)] from (zeroth-order) initial conditions $\mathbf{I}^c$ and $\boldsymbol{\alpha}$ at $t = 0$. The rms deviation ΔI_{rms} of the four intensities in Eq. (3.13) from $I(\text{AS})$ is used to provide some measure of the uncertainty in $I(\text{AS})$.

The method by which the individual intensities on the right-hand side of Eq. (3.13) are obtained and assessed for convergence for finite trajectory integration times is discussed in Appendix C. To extract the appropriate intensity from a classical Fourier spectrum of the dipole function, it is necessary to know the associated transition frequency. In the spectrum generated by the trajectory with actions $\mathbf{I}^c = \mathbf{I}(\mathbf{n}^c)$, the amplitude at $\boldsymbol{\Delta}\cdot\boldsymbol{\omega}^c$ will determine the semiclassical intensity for the transition specified by $(\mathbf{n},\boldsymbol{\Delta})$. The fundamental frequencies $\boldsymbol{\omega}^c$ of the correspondence trajectory can be determined by Fourier transforming the coordinates q_1, q_2, q_3 of the trajectory with actions $\mathbf{I}^c$. If the eigenvalues E and E' of the initial and final states are available, it is usually more convenient to locate the desired feature of the classical spectrum via the relationship $\boldsymbol{\Delta}\cdot\boldsymbol{\omega}^c \simeq \omega$, where $\omega = (E' - E)/\hbar$ is the exact transition frequency. Figure 4 shows the spectrum of μ_z for one of the four approximate eigentrajectories describing the state $(1\,0^0\,0)$. The particular peak indicated by the arrow is located at $\boldsymbol{\Delta}\cdot\boldsymbol{\omega}^c = (\omega_1^c,\omega_2^c,\omega_3^c)\cdot(2,0,0) = 2\omega_1^c$; further details are provided in the caption of Fig. 4.

It is also of interest to obtain semiclassical average values $\mu_z(\text{AS})$ of the dipole moment function for comparison to the corresponding quantum expectation value. (The average of μ_x is zero by symmetry in the x–y plane.) This is ac-

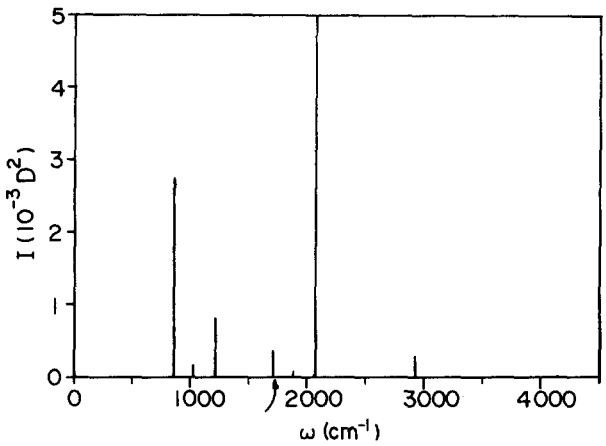

FIG. 4. Spectrum of the dipole moment function μ_z obtained from one of the four approximate eigentrajectories for the state (1 0° 0). The arrow below the abscissa indicates the peak whose area would provide the semiclassical intensity for the transition from (0 0° 0) to (2 0° 0) if arithmetic mean actions were used to specify the correspondence trajectory.

complished with the set of four trajectories used to generate $\overline{I}$, but with $\mathbf{I}^c$ replaced by $\mathbf{I} = \mathbf{I}(\mathbf{n})$, where $\mathbf{n}$ denotes a possible vibrational state (i.e., integer quantum numbers). The time average of μ_z, $\langle \mu_z \rangle_t$, was obtained for each trajectory and the average of the four $\langle \mu_z \rangle_t$ values yielded μ_z(AS).

C. Resonances

The first indication of the presence of nonlinear resonances in the present model for OCS came from the observation of some relatively large values of $\Delta E_{\rm rms}$ in the course of evaluating the semiclassical eigenvalues $\overline{E}$. A large $\Delta E_{\rm rms}$ value indicates that at least some of the ensemble of four adiabatically switched trajectories pass through resonant, or possibly even chaotic, zones of the phase space, but cannot provide a reliable indication of the resonant vs nonresonant character of the individual eigentrajectories which are assumed, under the adiabatic hypothesis, to be attained at $t = T'$. Since transition intensities are much more sensitive to the dynamical nature of the eigenstates than are the eigenvalues, identification and assessment of resonances in the approximate eigentrajectories used in our study is essential in establishing the utility of the present semiclassical method for intensities. Although relatively large values of $\Delta I_{\rm rms}$ were often found to be attributable to resonant approximate correspondence trajectories, the size of $\Delta I_{\rm rms}$ did not always prove to be a reliable signal for the occurrence of resonances. In order to unambiguously identify the occurrence of a resonance and to ascertain its dimensionality, its frequency ratio, its strength, and the phase space structure of the trajectory, we undertook the following analysis:

The quantitative aspect of our analysis relies on the recent and definitive work of Martens and Ezra who have developed a practical method for obtaining semiclassical actions, eigenvalues, and eigentrajectories for both nonresonant[18] and resonant[31] systems directly from the classical power spectra of the individual position coordinates. Tailoring their expression for the actions to the present notation and dimensionality yields

$$I_i = \sum_j G_{ij}\omega_j, \qquad i,j = 1,2,3 \tag{3.14}$$
$$G_{ij} = \sum_{\mathbf{k}} k_i |\mathbf{q}_{\mathbf{k}}|^2 k_j,$$

where ω_1, ω_2, and ω_3 are the fundamental frequencies as obtained from the Fourier transforms of the classical position variables $q_1(t)$, $q_2(t)$, and $q_3(t)$; $\mathbf{k} = (k_1,k_2,k_3)$ is a lattice vector with integer components; and $|\mathbf{q}_{\mathbf{k}}|^2 = q^2_{1,\mathbf{k}} + q^2_{2,\mathbf{k}} + q^2_{3,\mathbf{k}}$ is the sum of the intensities associated with the frequency $\mathbf{k}\cdot(\omega_1,\omega_2,\omega_3)$ in the spectra of the coordinates. Equation (3.14) is valid for both resonant and nonresonant classical motion, provided one recognizes that the actions I_i and the frequencies ω_i are associated with *different* sets of dynamical coordinates in each case.

For OCS, we applied Eq. (3.14) to a number of nonresonant and resonant approximate eigentrajectories. For the nonresonant cases, the fundamental frequencies are incommensurate and the actions I_i and frequencies ω_i are each associated with zeroth-order mode i. The energy is given by $E = (I_1,I_2,I_3)\cdot(\omega_1,\omega_2,\omega_3)$ and the quantization conditions are as given in Sec. III A:

$$I_1 = (n_1 + \tfrac{1}{2})\hbar, \quad I_2 = (n_2 + 1)\hbar,$$
$$I_3 = (n_3 + \tfrac{1}{2})\hbar, \quad \mathscr{L} = l\hbar. \tag{3.15}$$

Comparison of the actions I_i ($i = 1,2,3$) calculated numerically via Eq. (3.14) to those of Eq. (3.15) then provides a measure of the extent of breakdown of the adiabatic hypothesis for nonresonant cases. In general, there are numerous possibilities for a resonance in this system—rationally related frequencies for any of the three pairs of modes with the third mode being incommensurate, or rationally related frequencies for all three modes. Both types of resonance were observed in our study. Since the 4:1 resonance between modes 2 and 3 was found to be prevalent, all further results and discussion are confined to this case. The quantities I_1 and ω_1 have their usual meaning, but (I_2,I_3) and (ω_2,ω_3) are replaced by (I_2^r,I_3^r) and (ω_2^r,ω_3^r), where $\omega_2 = \omega_3/4 = \omega_2^r$. In phase space, ω_3^r gives the angular rate of rotation of points about an island on the surface of section and, in configuration space, it is the frequency of libration of the trajectory within the resonant caustics.[31] The numerical value of ω_3^r is obtained from the Fourier spectrum of q_2 or q_3 as the distance between the prominent peak at ω_2^r or $4\omega_2^r$, respectively, and the adjacent sideband. As pointed out by Martens and Ezra,[31] larger values of ω_3^r and concommitantly smaller values of the amplitude of the sideband indicate an increase in the "strength" of the resonance. The energy in the 4:1 case is given by $E = (I_1,I_2^r,I_3^r)\cdot(\omega_1,\omega_2^r,\omega_3^r)$ and the quantization conditions are

$$I_1 = (n_1 + \tfrac{1}{2})\hbar, \quad I_2^r = (n_2^r + 3)\hbar,$$
$$I_3^r = (n_3^r + \tfrac{1}{2})\hbar, \quad \mathscr{L} = l\hbar, \tag{3.16}$$

where $n_2^r = n_2 + 4n_3$.

The above analysis can be complemented, in qualitative fashion, by configuration space plots and surfaces of section

of the trajectories. We determined configuration space cross sections by the method of Noid *et al.*,[32] where intersections of the trajectory with each of three orthogonal planes are assigned to two-dimensional bins. The surfaces of section were determined by the method of Noid *et al.*[33]; e.g., the q_1–p_1 surface of section is specified by the conditions $q_2 = 0$, $|q_3| \leqslant \epsilon, p_2 \geqslant 0, p_3 \geqslant 0$, where ϵ is some small number chosen so as to compromise between obtaining a sufficient number of points and producing a curve with a narrow width.

IV. QUANTUM CALCULATION

Eigenvalues E_i and eigenvectors Ψ_i $(i = 1,2,3,...)$ for OCS were obtained variationally by diagonalizing $N \times N$ matrices of the Hamiltonian H [Eq. (2.1)] in a basis set of N wave functions ψ_i^0, in which the zeroth-order Hamiltonian H_0 is diagonal. Frequencies and intensities for the transition $i \rightarrow f$ are given by $(E_f - E_i)/\hbar$ and $|\langle \Psi_f | \mu_\beta | \Psi_i \rangle|^2$, respectively. The expectation value of the dipole moment function in state i is $\langle \Psi_i | \mu_\beta | \Psi_i \rangle$. These three quantities are used in Sec. V to provide an assessment of the semiclassical predications of Sec. III.

The basis set $\{\psi_i^0\}$ consists of wave functions which are products of harmonic oscillator wave functions ϕ_{n_1} and ϕ_{n_3} for modes 1 and 3, and polar wave functions[34] $\phi_{n_2,l}$ for mode 2:

$$\psi_i^0(q_1,q_2,q_3,\alpha_l) = \phi_{n_1}(q_1)\phi_{n_2,l}(q_2,\alpha_l)\phi_{n_3}(q_3), \qquad (4.1)$$

where i denotes a particular set of zeroth-order quantum numbers (n_1, n_2^l, n_3) and, for a given (positive) value of l, the allowed values of n_2 are l, $l+2$, $l+4$,.... Matrix elements of V [Eq. (2.8)] are analytic in this basis set. Evaluation of the matrix elements of T_v [Eq. (2.7)] is not straightforward and merits brief discussion. The quantum operator $\hat{T}_v$ is obtained by expanding the last equality of Eq. (2.7), while taking account of the noncommutivity of the conjugate pairs (q_1, p_1), (q_{2x}, p_{2x}), (q_{2y}, p_{2y}), (q_3, p_3). Operating on ψ_i^0 with $\hat{T}_v$ yields a (finite) linear combination of basis states

$$\hat{T}_v \psi_i^0 = \tfrac{1}{2}\mu \sum_j a_{ij} \psi_j^0. \qquad (4.2)$$

Determination of the matrix element $\langle \psi_k^0 | \hat{T}_v | \psi_i^0 \rangle$ is then reduced to evaluation of $\langle \psi_k^0 | \mu | \psi_j^0 \rangle$ for all j such that $a_{ij} \neq 0$. Since μ depends only on q_1 and q_3, its matrix elements are diagonal in n_2 and l. The remaining two-dimensional integral over q_1 and q_3 must be done numerically and we used 6×6 and 10×10 point Gauss–Hermite quadratures[35] for this purpose.

That l is a good quantum number for the OCS system is revealed by the block diagonal structure of the matrix of H with respect to l. Matrix diagonalizations were done for $l = 0$, 1, 2, 3, and 4; for each l value various basis set sizes were used in order to assess the convergence of the transition frequencies and intensities. The l-dependent basis set size is $N = (n_1^{\max} + 1) \times [(n_2^{\max} - l + 2)/2] \times (n_3^{\max} + 1)$, where $n_i^{\max}$ is the maximum value of the quantum number n_i permitted in mode i. The largest basis set had $(n_1^{\max}, n_2^{\max}, n_3^{\max}, l) = (10,16,7,0)$, giving $N = 792$.

V. NUMERICAL RESULTS AND DISCUSSION

This section is divided into four subsections for clarity of presentation. Section V A deals with the OCS energy levels, Sec. V B with the transition intensities, and Sec. V C with dipole moment average values. Analysis of resonant and nonresonant approximate eigentrajectories is the subject of Sec. V D.

A. Energy levels

In this subsection, energy levels obtained semiclassically, quantum mechanically, and experimentally are presented and compared. All levels are reported, in Table III, as transition frequencies from the ground state. The first column of Table III labels the level according to its zeroth-order quantum numbers. The semiclassical results $E(\mathrm{AS}) = \overline{E}(n_1 n_2^l n_3) - \overline{E}(0\,0^0\,0)$ and $\Delta E(\mathrm{AS}) = [\Delta E^2_{\mathrm{rms}}(n_1 n_2^l n_3) + \Delta E^2_{\mathrm{rms}}(0\,0^0\,0)]^{1/2}$ are given in columns 2 and 3. The corresponding quantum levels $E(\mathrm{Q})$ (see Sec. IV), the experimental levels $E(\mathrm{exp})$ reported in Ref. 16, and the semiclassical levels $E(\mathrm{Col})$ of Colwell[10] are listed in columns 4, 6, and 8, respectively. The differences $\delta E_1 = E(\mathrm{AS}) - E(\mathrm{Q})$ and $\delta E_2 = E(\mathrm{AS}) - E(\mathrm{exp})$ are listed in columns 5 and 7, respectively.

Since assessment of the present semiclassical results relies to a large extent on comparison to the quantum results, it is appropriate to comment first on the accuracy of the quantum energy levels. All $E(\mathrm{Q})$ values are reported to the nearest 0.1 cm^{-1} in Table III and are converged within 0.1 cm^{-1} unless otherwise noted; the first $\sim$20 levels for each l value are converged within 0.02 cm^{-1}. The set of 145 converged levels in Table III represents the largest available set of quantum levels to date for the OCS system as specified in Sec. II A. It is of interest to compare our quantum levels to those of FSW,[14] since the latter have been compared to the semiclassical predictions of two earlier OCS studies.[9,10] FSW used smaller basis sets, the largest one having 200 elements. The basis functions were, however, judiciously chosen to include all levels directly coupled to the states whose eigenvalues were being sought. Since the FSW prediction for the ground state energy differs from ours by only 0.02 cm^{-1} (1999.40 vs 1999.38 cm^{-1}), any discrepancies between the two sets of levels are attributable to differences in the absolute eigenvalues of the states whose energy levels relative to the ground state are being compared. Comparison of the 68 FSW levels $E(\mathrm{FSW})$ to the present $E(\mathrm{Q})$ values revealed the following: in all but one case, $E(\mathrm{Q}) < E(\mathrm{FSW})$. For the first $\sim$12 levels of each l value, the difference $E(\mathrm{FSW}) - E(\mathrm{Q})$ was $< \sim 0.5$ cm^{-1}, while for many of the higher levels, it was 1–3 cm^{-1}. Several of the FSW levels were found to be unconverged; noteworthy are $(1\,6^0\,0)$, $(2\,5^1\,0)$, and $(1\,7^1\,0)$ for which $E(\mathrm{FSW})$ exceeds $E(\mathrm{Q})$ by 11.2, 5.1, and 14.3 cm^{-1}, respectively.

An assessment of the semiclassical results $E(\mathrm{AS})$ is provided below by comparison to $E(\mathrm{Q})$, $E(\mathrm{exp})$, and $E(\mathrm{Col})$. The 176 values of $E(\mathrm{AS})$ in Table III represent the largest available set of semiclassical levels for the OCS system as specified in Sec. II A, consisting of 59, 49, 47, 20, and 1 levels for $l = 0$, 1, 2, 3, and 4, respectively. We begin by examining

TABLE III. Semiclassical, quantum, and experimental OCS transition frequencies (in cm^{-1}) from the ground state ($0\,0^0\,0$).

Level	E(AS)[a]	ΔE(AS)[b]	E(Q)[c]	δE_1[d]	E(exp)[e]	δE_2[f]	E(Col)[g]
$l=0$							
10^00	859.2	0.41	859.0	0.2	859.0	0.2	859.3
02^00	1046.9	0.76	1046.9	0.0	1047.0	−0.1	1046.8
20^00	1710.9	0.36	1710.6	0.3	1711.1	−0.2	1710.7
12^00	1891.7	1.64	1892.0	−0.3	1892.2	−0.5	1893.3
00^01	2062.1	0.71	2062.0	0.1	2062.2	−0.1	2062.7
04^00	2105.7	1.19	2105.8	−0.1	2104.8	0.9	2105.2
30^00	2555.4	0.36	2554.9	0.5	2556.0	−0.6	2554.8
22^00	2730.2	2.42	2730.6	−0.4	2731.4	−1.2	2730.8
10^01	2918.4	0.38	2918.1	0.3	2918.1	0.3	2919.3
14^00	2935.7	1.36	2935.9	−0.2	2937.2	−1.5	2935.4
02^01	3094.5	4.46	3095.0	−0.5	3095.6	−1.1	3095.2
06^00	3174.9	1.82	3175.4	−0.5	3170.6	4.3	3173.9
40^00	3393.0	0.36	3392.5	0.5	3394.0	−1.0	3392.0
32^00	3563.0	2.02	3562.9	0.1	3564.5	−1.5	3564.1
24^00	3760.4	1.76	3759.4	1.0	3762.8	−2.4	3759.6
20^01	3767.2	0.36	3767.6	−0.4	3768.5	−1.3	3767.9
12^01	3937.1	4.19	3937.2	−0.1	3937.4	−0.3	3938.5
16^00	3988.9	1.77	3989.0	−0.1			3988.3
00^02	4101.6	0.64	4101.4	0.2	4101.4	0.2	4103.8
04^01	4140.4	5.15	4141.0	−0.6	4141.2	−0.8	4141.3
50^00	4224.2	0.36	4224.6	−0.4	4224.9	−0.7	4222.6
08^00	4253.6	2.80	4254.6	−1.0			4255.2
42^00	4389.9	1.21	4389.5	0.4	4391.4	−1.5	4390.5
34^00	4576.8	5.66	4578.7	−1.7			
30^01	4609.0	0.35	4608.9	0.1	4609.9	−0.9	4609.2
22^01	4773.2	3.09	4772.4	0.8	4773.2	0.0	4775.4
26^00	4797.3	1.26	4798.3	−1.0			
10^02	4954.7	0.38	4954.3	0.4	4953.9	0.8	4958.4
14^01	4967.6	5.59	4968.8	−1.2	4970.4	−2.8	
18^00	5050.1	2.98	5050.4	−0.3			
60^00	5049.5	0.76	5057.3[h]	−7.8			5047.1
02^02	5118.7	8.22	5117.9	0.8	5121.0	−2.3	5119.6
06^01	5198.3	6.09	5198.7	−0.4	5196.0	2.3	
52^00	5210.9	0.98	5212.1	−1.2			
010^00	5341.0	3.72	5342.5	−1.5			
44^00	5389.3	8.04	5393.0	−3.7			
40^01	5444.0	0.36	5444.5	−0.5	5445.0	−1.0	5443.2
36^00	5601.9	5.79	5596.7	5.2			
32^01	5604.2	1.15	5607.8	−3.6	5602.5	1.7	5610.3
24^01	5786.6	4.32	5788.9	−2.3	5792.0	−5.4	
20^02	5800.5	0.36	5801.3	−0.8	5801.9	−1.4	5804.6
28^00	5840.0	1.77	5842.8[i]	−2.8			
12^02	5960.5	5.99	5957.3	3.2	5959.3	1.2	
16^01	6009.5	4.64	6010.1	−0.6			
110^00	6117.8	4.27	6118.6	−0.8			
00^03	6118.3	0.44	6119.1[i]	−0.8	6117.6	0.7	
04^02	6146.1	16.15	6148.9	−2.8	6154.7	−8.6	
54^00	6200.7	7.10	6205.3	−4.6			
08^01	6266.8	6.25	6266.7	0.1			
46^00	6402.9	9.65	6400.6[h]	2.3			
42^01	6427.9	0.52	6429.4	−1.5			
012^00	6436.1	6.62	6438.3[h]	−2.2			
34^01	6599.8	6.23	6603.5	−3.7			
38^00	6633.1	2.84	6633.2[i]	−0.1			
30^02	6639.4	0.35	6640.2[h]	−0.8	6640.1	−0.7	
22^02	6794.7	3.52	6789.4[h]	5.3	6791.6	3.1	
26^01	6815.8	4.93	6816.8[h]	−1.0			
210^00	6893.2	2.27	6893.8[h]	−0.6			
10^03	6968.2	0.36	6968.0[h]	0.2	6966.2	2.0	6978.4
$l=1$							
01^10	520.3	0.74	520.3	0.0	520.4	−0.1	520.3
11^10	1372.9	0.93	1372.8	0.1			1373.0
03^10	1573.4	0.96	1573.4	0.0	1573.4	0.0	1573.2
21^10	2218.5	0.72	2218.2	0.3			2218.6
13^10	2411.4	0.41	2411.3	0.1	2412.2	−0.8	2411.4
01^11	2575.3	2.02	2575.1	0.2	2575.3	0.0	2575.4
05^10	2637.6	1.41	2637.8	−0.2	2635.6	2.0	2636.9

TABLE III (*continued*).

Level	E(AS)[a]	ΔE(AS)[b]	E(Q)[c]	δE_1[d]	E(exp)[e]	δE_2[f]	E(Col)[g]
31^10	3057.4	0.46	3056.9	0.5	3057.1	0.3	3057.0
23^10	3242.3	3.01	3243.1	−0.8	3245.3	−3.0	3245.9
11^11	3425.3	1.42	3424.6	0.7	3424.1	1.2	3424.9
15^10	3459.8	1.08	3460.1	−0.3			3459.5
03^11	3614.4	4.70	3614.8	−0.4	3615.4	−1.0	3165.0
07^10	3711.9	2.13	3712.4	−0.5			3711.3
41^10	3889.9	0.40	3889.3	0.6	3889.6	0.3	3889.1
33^10	4067.8	4.74	4069.1	−1.3	4072.7	−4.9	
21^11	4268.1	0.52	4266.4	1.7	4266.3	1.8	4268.8
25^10	4276.7	2.79	4277.6	−0.9			
13^11	4448.9	5.22	4450.0	−1.1	4450.8	−1.9	4456.9
17^10	4517.1	2.61	4517.5	−0.4			4515.7
01^12	4607.9	3.02	4606.0	1.9	4607.1	0.8	4608.5
05^11	4666.8	5.21	4666.9	−0.1	4666.1	0.7	4667.4
51^10	4716.3	0.47	4716.3	0.0			4715.1
09^10	4795.6	3.08	4796.1	−0.5			
43^10	4889.3	3.70	4889.8	−0.5			
35^10	5089.7	4.47	5087.8	1.9			
31^11	5103.9	0.40	5104.1	−0.2			5104.1
23^11	5277.4	4.67	5278.7	−1.3	5280.5	−3.1	5281.2
27^10	5318.2	1.83	5318.6	−0.4			5316.5
11^12	5454.1	1.59	5452.4[i]	1.7	5452.5	1.6	
15^11	5486.2	4.99	5486.9	−0.7			
61^10	5537.1	0.77	5542.0	−4.9			5535.9
19^10	5582.9	2.80	5582.7	0.2			
03^12	5628.2	11.94	5630.0	−1.8	5634.2	−6.0	5632.0
53^10	5705.4	2.33	5707.2	−1.8			
07^11	5729.8	6.25	5730.0	−0.2			
011^10	5887.1	4.22	5888.1	−1.0			
45^10	5891.9	8.73	5895.9	−4.0			
41^11	5933.4	0.40	5933.8	−0.4			5933.1
33^11	6100.6	6.65	6099.5	1.1			
37^10	6113.7	4.94	6117.6	−3.9			
21^12	6292.9	0.59	6290.7[i]	2.2	6290.9	2.0	6297.3
25^11	6299.5	4.23	6301.8	−2.3			
29^10	6364.0	1.28	6366.3[i]	−2.3			
13^12	6461.7	9.62	6462.5[i]	−0.8	6466.1	−4.4	
17^11	6531.0	4.64	6531.6	−0.6			
01^13	6615.7	3.01	6613.5[h]	2.2	6615.8	−0.1	
111^10	6653.9	4.62	6654.3[h]	−0.4			
05^12	6665.3	15.02	6667.6[i]	−2.3			
11^13	7457.6	1.04			7457.4	0.2	
$l=2$							
02^20	1040.8	0.50	1040.8	0.0			1040.8
12^20	1886.7	0.92	1886.8	−0.1			1889.1
04^20	2099.8	1.05	2099.8	0.0			2099.4
22^20	2726.3	1.41	2726.3	0.0			2726.7
14^20	2930.6	1.18	2930.6	0.0			2930.4
02^21	3088.6	2.42	3088.6	0.0	3088.8	−0.2	3088.9
06^20	3169.4	1.98	3169.6	−0.2			3168.4
32^20	3559.8	1.17	3559.4	0.4			3560.8
24^20	3755.9	1.50	3755.8	0.1	3759.7	−3.8	3756.9
12^21	3932.0	2.42	3931.7	0.3			3932.7
16^20	3983.6	1.36	3984.0	−0.4			3982.2
04^21	4134.6	4.33	4134.8	−0.2			4135.1
08^20	4248.4	2.85	4248.9	−0.5			4248.1
42^20	4387.2	0.76	4386.6	0.6			4389.1
34^20	4573.6	4.68	4575.4	−1.8			
22^21	4769.0	1.83	4767.9	1.1			4774.0
26^20	4793.0	1.11	4793.8	−0.8			
14^21	4962.8	4.32	4963.1	−0.3			
18^20	5044.5	2.44	5045.5	−1.0			
02^22	5112.5	5.08	5111.3	1.2	5113.2	−0.7	5112.7
06^21	5192.3	5.23	5192.7	−0.4			
52^20	5208.9	0.70	5208.6	0.3			
010^20	5336.1	3.90	5337.0	−0.9			
44^20	5387.3	6.96	5390.2	−2.9			
36^20	5598.0	5.50	5593.9	4.1			
32^21	5599.9	0.75	5602.8	−2.9			

Table III (*continued*).

Level	$E(AS)^a$	$\Delta E(AS)^b$	$E(Q)^c$	$\delta E_1{}^d$	$E(exp)^e$	$\delta E_2{}^f$	$E(Col)^g$
24^21	5783.2	3.38	5785.1	− 1.9			
28^20	5837.5	2.23	5838.5	− 1.0			
12^22	5953.9	3.99	5951.3[i]	2.6	5952.1	1.8	
16^21	6005.1	5.00	6004.8	0.3			
62^20	6025.2	0.67	6028.2	− 3.0			
110^20	6112.5	3.06	6114.2	− 1.7			
04^22	6141.4	12.33	6142.3	− 0.9			
54^20	6199.1	6.13	6202.0	− 2.9			
08^21	6261.5	7.09	6260.9	0.6			
46^20	6399.9	9.63	6398.1	1.8			
42^21	6424.0	0.39	6424.5	− 0.5			6428.5
012^20	6429.6	4.98	6432.9	− 3.3			
34^21	6597.4	5.89	6600.3	− 2.9			
38^20	6628.4	4.02	6629.2	− 0.8			
22^22	6787.6	2.16	6784.3[i]	3.3			
26^21	6811.2	4.33	6811.3[i]	− 0.1			
210^20	6888.6	3.71	6889.2[i]	− 0.6			
14^22	6966.7	10.62	6968.2[i]	− 1.5			
18^21	7056.1	7.87	7055.0[i]	1.1			
02^23	7114.9	7.65	7109.3[h]	5.6			
06^22	7184.4	14.91	7186.0[i]	− 1.6			
$l = 3$							
03^30	1561.4	0.55	1561.5	− 0.1			1561.4
13^30	2401.1	0.36	2401.1	0.0			2401.2
05^30	2625.9	1.12	2626.1	− 0.2			2625.6
23^30	3234.3	1.34	3234.7	− 0.4			3237.2
15^30	3449.7	0.85	3449.9	− 0.2			3449.7
03^31	3602.5	2.13	3602.5	0.0			
07^30	3700.5	1.84	3700.9	− 0.4			
33^30	4062.1	2.22	4062.4	− 0.3			
25^30	4268.0	2.18	4268.4	− 0.4			
13^31	4439.3	2.15	4439.3	0.0			4438.5
17^30	4507.2	2.33	4507.6	− 0.4			
05^31	4654.9	4.04	4654.8	0.1			
09^30	4784.4	2.93	4784.9	− 0.5			
43^30	4884.7	1.77	4884.7[h]	0.0			
35^30	5082.1	4.04	5081.9[h]	0.2			
23^31	5269.8	2.26	5269.7	0.1			
27^30	5309.5	1.73	5310.0[i]	− 0.5			
15^31	5476.0	3.82	5476.2	− 0.4			
19^30	5573.0	2.71	5573.0	0.0			
03^32	5617.7	5.21	5617.3[i]	0.4	5619.7	− 2.0	5618.7
$l = 4$							
04^40	2082.0	0.55	2082.1	0.1			2082.9

[a] Semiclassical levels via adiabatic switching of four trajectories, as described in the text, and relative to the ground state energy of 1998.1 cm^{-1}.
[b] Root-mean-squared deviation of $E(AS)$ as defined in the text.
[c] Quantum levels, relative to ground state energy of 1999.4 cm^{-1}.
[d] $E(AS) - E(Q)$.
[e] Experimental levels reported in Ref. 16.
[f] $E(AS) - E(exp)$.
[g] Semiclassical levels of Colwell (Ref. 10), relative to the ground state energy of 1998.1 cm^{-1}.
[h] Not converged within 1.0 cm^{-1}.
[i] Converged within 1.0 cm^{-1} but not within 0.1 cm^{-1}.

the agreement between the semiclassical and the 145 converged quantum levels since these two sets of results are derived from the same Hamiltonian. The magnitude of the largest deviation $|\delta E_1|$ of an $E(AS)$ value from an $E(Q)$ value is 5.2 cm^{-1} for the state $(3\,6^0\,0)$. In 112 of 145 cases, $|\delta E_1| \leqslant 1.0\ cm^{-1}$ and in 128 cases $|\delta E_1| \leqslant 2.0\ cm^{-1}$. In 134 of 145 cases, $\Delta E(AS) \geqslant |\delta E_1|$, indicating that the uncertainty in the semiclassical levels quite reliably provides an upper bound on the difference between $E(AS)$ and the desired quantity $E(Q)$. The agreement between the semiclassical levels and the 64 available experimentally determined levels was assessed in similar fashion. Since the approximate potential energy function used in the theoretical calculations introduces an additional source of error, the agreement is not expected to be as good as for $E(Q)$. In 49 of 64 cases, $|\delta E_2| \leqslant 2.0\ cm^{-1}$ and in 41 cases $\Delta E(AS) \geqslant |\delta E_2|$, again indicating the utitility of $\Delta E(AS)$ in bounding the discrepancy between $E(AS)$ and the actual value. Of the 15 levels on the

range 5500–7500 cm^{-1} above the ground state, 11 have $|\delta E_2| \leqslant 2.0$ cm^{-1}. This suggests that the potential energy function is reasonably accurate at energies in excess of those used in the original fitting procedure by FSW. The highest experimental level considered by these authors was $(1\ 1^1\ 2)$ at ~ 5453 cm^{-1} above the ground state. Of the 84 semiclassical levels $E(\mathrm{Col})$ in Table III, 70 of them differ from $E(\mathrm{AS})$ by 2 cm^{-1} or less.

It is interesting to note, in Table III, that there are some levels having $\Delta E(\mathrm{AS}) \gg |\delta E_1|$ which nevertheless agree with $E(\mathrm{Q})$ to within 1 cm^{-1}, e.g., $(0\ 2^0\ 2)$ and $(1\ 5^1\ 1)$. Large values of $\Delta E(\mathrm{AS})$ indicate breakdown of the adiabatic assumption and are presumably attributable, at these energies, to passage of some or all of the four trajectories through resonant regions of phase space during the switching process. The fortuitous cancellation of nonadiabatic effects in calculating the eigenvalues $\bar{E}$ [and hence $E(\mathrm{AS})$] in many of the larger $\Delta E(\mathrm{AS})$ cases is reassuring, since this provided the original motivation[7] for using ensemble averages rather than single trajectory results in the ASM. In an attempt to reduce the uncertainty $\Delta E(\mathrm{AS})$, we applied the suggestion offered in Ref. 7 to a few of the states in Table III. To avoid resonances encountered *during* switching, as opposed to one present in H_0, the proposal is to retain H_0, but break up the coupling term H_1 and then switch on its parts at different rates, viz.,

$$H_I = \sum_i H_i, \quad H(t) = H_0 + \sum_i \lambda_i(t) H_i. \tag{5.1}$$

Not knowing the strength or location of resonance zones in the phase space, a trial and error approach was taken in the choice of pathways. We tried switching on the individual terms of H_I [Eqs. (2.6)–(2.8)] sequentially at the same rate and simultaneously at different rates, but were unable to improve the energies $E(\mathrm{AS})$ or to reduce the uncertainties $\Delta E(\mathrm{AS})$ in a systematic fashion.

B. Transition intensities

Semiclassical and quantum intensities for transitions from the ground state, from two states with one mode singly excited, and from a highly excited bending state are compared in Table IV. As in Sec. V A, the initial and final states are labeled by their zeroth-order quantum numbers. The semiclassical intensity $I(\mathrm{AS})$ in column 3 and associated uncertainty $\Delta I(\mathrm{AS})$ in column 4 were obtained from Eq. (3.13) with correspondence actions determined by Eq.

TABLE IV. Semiclassical and quantum transition intensities of OCS.

Initial state	Final state	$I(\mathrm{AS})$[a] (D^2)	$\Delta I(\mathrm{AS})$[b] (%)	$I(\mathrm{Q})$[a] (D^2)	δI[c] (%)	N_{res}[d]
00^00	10^00	3.06(3)	11.7	3.80(3)	−19.5	4
	02^00	8.43(4)	12.9	8.47(4)	−0.5	
	20^00	5.78(4)	4.0	5.95(4)	−2.9	
	12^00	3.16(4)	51.5	4.00(4)	−21.0	2
	00^01	1.48(1)	5.2	1.49(1)	−0.7	
	04^00	5.22(4)	3.0	4.94(4)	5.7	
	22^00	5.29(6)	5.6	6.86(6)	−22.9	4
	10^01	4.95(4)	13.7	7.83(4)	−36.8	4
	02^01	9.31(5)	19.6	9.80(5)	−5.0	
	00^02	2.84(4)	5.2	3.12(4)	−9.0	3
	04^01	1.59(6)	4.6	1.61(6)[e]	−1.2	
	01^10	1.17(3)	6.7	1.17(3)	0.0	
	11^10	3.91(7)	8.2	3.98(7)	−1.8	
10^00	20^00	8.66(3)	0.1	8.71(3)	−0.6	
	30^00	1.64(3)	0.2	1.65(3)	−0.6	
	10^01	1.44(1)	1.6	1.44(1)	0.0	
	12^00	9.99(4)	45.6	1.06(3)	−5.8	4
	22^00	9.36(4)	26.2	6.50(4)[e]	44.0	3
01^10	11^10	3.32(3)	2.1	3.41(3)	−2.6	
	03^10	1.57(3)	4.0	1.62(3)	−3.1	
	13^10	7.74(4)	7.1	7.75(4)	−0.1	
	01^11	1.46(1)	5.6	1.46(1)	0.0	
	11^11	6.72(4)	11.2	7.28(4)[e]	−7.7	2
	21^10	3.90(4)	11.2	4.89(4)	−20.3	2
	05^10	6.96(4)	3.0	6.72(4)	3.6	
03^30	03^32	3.26(4)	4.3	3.29(4)	0.9	

[a] The number in parentheses is the negative of the power of 10, e.g., $3.06(3) = 3.06 \times 10^{-3}$.
[b] $\Delta I(\mathrm{AS}) = \Delta I_{rms}/I(\mathrm{AS}) \times 100\%$.
[c] $\delta I = [I(\mathrm{AS}) - I(\mathrm{Q})]/I(\mathrm{AS}) \times 100\%$.
[d] The number of correspondence trajectories found to display a 4:1 resonance between modes 2 and 3. No entry indicates the absence of resonant trajectories in the ensemble of four correspondence trajectories.
[e] Converged within five in the third figure; all other $I(\mathrm{Q})$ entries converged within one in the third figure.

(3.11) for modes 1 and 3, by Eq. (3.12) for mode 2 when $\Delta l = 0$, and by Eq. (3.10) for mode 2 when $\Delta l = 1$. On the basis of the examination of the dipole spectra of selected trajectories in Appendix C, the $I(\mathrm{AS})$ values are expected to be converged to three significant figures. The quantum intensities $I(\mathrm{Q})$ in column 5 were obtained as described in Sec. IV and are converged within one unit in the third figure unless otherwise indicated in Table IV. The quantity δI in column 6 is the difference $I(\mathrm{AS})$–$I(\mathrm{Q})$. The number N_{res} of resonant correspondence trajectories contributing to $I(\mathrm{AS})$ is listed in column 7. The classification of the four correspondence trajectories as resonant or nonresonant was accomplished by application of the Fourier analysis of the coordinates described in Sec. III C. In all cases, the resonance was found to be 4:1 between modes 2 and 3.

To begin the discussion of the data in Table IV, we first consider only those semiclassical intensities determined by an ensemble of (four) nonresonant trajectories, i.e., $N_{\mathrm{res}} = 0$. Under this condition, the maximum absolute discrepancy $|\delta I|$ is seen to be 5.7% and, in 13 of 17 cases, the agreement is within 3%. In 14 of 17 cases, $\Delta I(\mathrm{AS}) \gtrsim |\delta I|$ indicating that $\Delta I(\mathrm{AS})$ usually provides an approximate upper bound on the difference between $I(\mathrm{AS})$ and $I(\mathrm{Q})$. Note, however, that $\Delta I(\mathrm{AS})$ ranges over two orders of magnitude for the nonresonant ensembles of trajectories, indicating the sensitivity of intensity results to trajectory initial conditions when approximate eigentrajectories are used. For several nonresonant cases in Table IV, $\Delta I(\mathrm{AS})$ is comparable to or exceeds that associated with some of the resonance cases.

In the absence of resonant correspondence trajectories, it is possible to reliably assess the influence of the various correspondence rules given in Sec. III B on the agreement with the quantum results. This is done in Table V, where two semiclassical transition intensities $I_i(\mathrm{AS})$ and associated transition frequencies $\omega_i(\mathrm{AS})$ $(i = 1,2)$ are compared to the corresponding quantum quantities $I(\mathrm{Q})$ and $\omega(\mathrm{Q})$ for selected $\Delta l = 0$ transitions in Table IV. Also listed in Table V B are semiclassical frequencies $\omega(\mathrm{AS})$, which are differences between initial and final energy levels $E(\mathrm{AS})$. $I_1(\mathrm{AS})$ is obtained via Eq. (3.13) with arithmetic mean values [Eq. (3.10)] for n_1^c, n_2^c, n_3^c, whereas $I_2(\mathrm{AS})$ results from the use of geometriclike mean values [Eq. (3.11) for modes 1 and 3 and Eq. (3.12) for mode 2] and is the same as $I(\mathrm{AS})$ in Table IV. The frequency $\omega_i(\mathrm{AS})$ is the average of the positions $\mathbf{\Delta}\cdot\boldsymbol{\omega}^c$ of the spectral peaks whose area determines $I_i(\mathrm{AS})$. The best agreement with $I(\mathrm{Q})$ is clearly provided by $I_2(\mathrm{AS}) = I(\mathrm{AS})$ thus motivating the use of the $i = 2$ results throughout Table IV. In general, $I_1(\mathrm{AS})$ overestimates $I(\mathrm{Q})$. Noteworthy is the advantage of using the new correspondence rule Eq. (3.12) for mode 2 instead of Eq. (3.11) as might have otherwise been adopted. Since Eq. (3.12) reduces to the arithmetic mean for $\Delta_2 = 2$ transitions, we have replaced $I_1(\mathrm{AS})$ by a quantity $I_1'(\mathrm{AS})$ for the two $\Delta_2 = 2$ transitions in Table V. The latter intensity is obtained using the geometriclike mean of Eq. (3.11) for mode 2 and is given in parentheses in the $I_1(\mathrm{AS})$ column. $I_1'(\mathrm{AS})$ is seen to underestimate $I(\mathrm{Q})$ in both cases. The frequencies $\omega_1(\mathrm{AS})$ are not as accurate as $\omega(\mathrm{AS})$ in predicting $\omega(\mathrm{Q})$, although they are certainly accurate enough to permit reliable identification of the required spectral peak. In any case, the transition frequencies $\omega(\mathrm{AS})$ are much easier to evaluate numerically, involving the adiabatic switching for $70\tau_{\mathrm{avg}}$ of two groups of four trajectories vs integrating four correspondence trajectories for $1965\,\tau_{\mathrm{avg}}$.

TABLE V. (A) Comparison of correspondence rules for transition intensities.[a] (B) Comparison of correspondence rules for transition frequencies.[b]

(A) Initial state	Final state	$I_1(\mathrm{AS})$[c]	$I_2(\mathrm{AS})$[d]	$I(\mathrm{Q})$
00^00	20^00	6.57(4)	5.78(4)	5.95(4)
	02^00	[7.76(4)]	8.43(4)	8.47(4)
	04^00	5.63(4)	5.22(4)	4.94(4)
	02^01	[8.54(5)]	9.31(5)	9.80(5)
	04^01	1.59(6)	1.59(6)	1.61(6)
10^00	30^00	1.70(3)	1.64(3)	1.65(3)
01^10	05^10	7.34(4)	6.97(4)	6.72(4)

(B) Initial state	Final state	$\omega_1(\mathrm{AS})$[e]	$\omega_2(\mathrm{AS})$[f]	$\omega(\mathrm{AS})$[g]	$\omega(\mathrm{Q})$[h]
00^00	20^00	1711.4	1712.4	1710.9	1710.6
	02^00	[1046.9]	1047.6	1046.9	1046.9
	04^00	2107.6	2103.9	2105.7	2105.8
	02^01	[3096.7]	3096.7	3094.5	30995.0
	04^01	4098.8	4142.4	4140.4	4141.0
10^00	30^00	1697.1	1697.9	1696.2	1695.9
01^10	05^10	2119.1	2117.7	2117.3	2117.5

[a] Intensities in (Debye)^2; number in parentheses after each intensity is negative of the power of ten.
[b] Frequencies in cm^{-1}.
[c] Obtained from trajectories with arithmetic mean actions [Eq. (3.10)].
[d] Obtained from trajectories with geometriclike mean actions [Eq. (3.11) for modes 1 and 3, Eq. (3.12) for mode 2].
[e] Obtained from trajectories with arithmetic mean actions [Eq. (3.10)].
[f] Obtained from trajectories with geometriclike mean actions [Eq. (3.11) for modes 1 and 3, Eq. (3.12) for mode 2].
[g] Difference of semiclassical energies $E(\mathrm{AS})$.
[h] Difference of quantum energies $E(\mathrm{Q})$.

For transitions whose semiclassical intensity is determined in whole or in part by resonant correspondence trajectories, the agreement between $I(\mathrm{AS})$ and $I(\mathrm{Q})$ is generally poor compared to the nonresonant cases. This is to be expected on the basis of the discussion following Eq. (3.9) in Sec. III B. In all but one of the nine resonance cases, $|\delta I|$ exceeds 6%, reaching a maximum of 44%. The $\Delta I(\mathrm{AS})$ values are larger, on the average, for the resonant than for the nonresonant cases but, nevertheless, in only three of nine resonance cases is $\Delta I(\mathrm{AS}) > |\delta I|$. We note that $I(\mathrm{AS}) < I(\mathrm{Q})$ in all but one resonance case and that only the principal peak in the resonant spectrum was used in the determination of the $I(\mathrm{AS})$ entries in Table IV. Since the resonance sidebands merge with the principal peak in the nonresonant limit, the above observation suggests the inclusions of sidebands in the intensity computation as an *ad hoc* correction. This tacitly assumes that the initial and final states involved in the transition are described semiclassically by nonresonant (exact) eigentrajectories. Whether this is actually the case for any of the vibrational states of our model of OCS

is not known and lies beyond the scope of this study. Including the immediately adjacent sidebands reduced $|\delta I|$ to $\leqslant$ 6% in only four of nine cases and in two of the remaining five cases *increased* the discrepancy by over estimating $I(Q)$. The lack of a rigorous justification for the correction and the fact that it does not systematically improve our semiclassical results, indicate that further study is needed if resonant trajectories are somehow to be interpreted within the context of the *primitive* semiclassical theory of intensities.

We conclude this subsection with a comment on the applicability of the semiclassical method to transitions involving a change in l from 0 to 1, 2, 3,... etc. In zeroth order, the classical motion of mode 2 when $l = 0$ is here described by a 1D periodic trajectory, whereas a precessing trajectory is used for $l \neq 0$. Since l is a constant of the motion for the full Hamiltonian, the topology of the mode 2 motion will be preserved under the influence of the coupling to modes 1 and 3. As has been discussed in Ref. 4, the tori for these two types of motion are topologically inequivalent and the primitive semiclassical approach to intensities is expected to be invalidated. The $I(AS)$ values for the two transitions with $\Delta l = 1$ in Table IV are seen, however, to be in excellent agreement with $I(Q)$. Both $I(AS)$ values were obtained from trajectories with mode 2 correspondence "quantum" numbers of $n_2^c = \frac{1}{2}$ and $l^c = \frac{1}{2}$, indicating that the correspondence trajecatories are of the precessing type. The success of the semiclassical approach is fortuitous in the sense that it resides in a feature of the $l = 0$ wave functions, namely that they have circular symmetry about the molecular axis. As such, these wave functions probably more closely correspond to trajectories with small but nonzero l. We reevaluated some of our $E(AS)$ and $I(AS)$ results with l equal to several small positive numbers and obtained essentially the same values as with $l = 0$. Insensitivity of the eigenvalues of the Hénon–Heiles system to small changes in the angular momentum action has been noted by Noid and Marcus.[25] The use of a periodic trajectory in zeroth order for mode 2 when $l = 0$ was not found to result in semiclassical levels $E(AS)$ which are in worse (or better) agreement with $E(Q)$ than the $E(AS)$ results for $l = 1,2$, or 3.

C. Dipole moment

In Table VI, semiclassical dipole moment averages $\mu_z(AS)$ obtained from a set of four approximate eigentrajectories (see the end of Sec. III B) are compared to the quantum values $\mu_z(Q)$ for 13 selected OCS vibrational states. For all but two states, the agreement, as measured by $\delta\mu_z = \mu_z(AS) - \mu_z(Q)$, is within 0.003 D. For all but one state ($2\,2^0\,0$), the rms deviation $\Delta\mu_z(AS)$ about $\mu_z(AS)$ provides an upper bound on the absolute value $|\delta\mu_z|$ of the discrepancy. The range in the uncertainty $\Delta\mu_z(AS)$ for these 13 states indicates that $\mu_z(AS)$, like $I(AS)$, is sensitive to the accuracy of the approximate eigentrajectory used to determine it. No attempt was made to classify as resonant or nonresonant each of the four trajectories contributing to each $\mu_z(AS)$ value in Table VI.

TABLE VI. Semiclassical and quantum dipole moment averages for selected states of OCS.[a]

State	$\mu_z(AS)$	$\Delta\mu_z(AS)$	$\mu_z(Q)$	$\delta\mu_z$[b]
00^00	0.7105	0.0032	0.7095	0.0010
10^00	0.6887	0.0013	0.6890	−0.0005
02^00	0.6880	0.0011	0.6877	0.0003
20^00	0.6680	0.0002	0.6677	0.0003
12^00	0.6767	0.0107	0.6675	0.0092
00^01	0.7400	0.0037	0.7427	−0.0027
04^00	0.6663	0.0013	0.6661	0.0002
22^00	0.6359	0.0020	0.6467	−0.0108
01^10	0.6990	0.0018	0.6987	0.0003
03^10	0.6771	0.0011	0.6768	0.0003
21^10	0.6556	0.0033	0.6573	−0.0017
02^20	0.6882	0.0006	0.6880	0.0002
14^20	0.6472	0.0021	0.6464	0.0008

[a] All entries in Debye.
[b] $\mu_z(AS) - \mu_z(Q)$.

D. Analysis of trajectories

Two different kinds of analysis were undertaken in order to elucidate various features of nonresonant and resonant approximate eigentrajectories—numerical determination of the actions and pictorial representations of the phase space structure.

1. Determination of actions

During the switching process, nonadiabatic effects are expected to result in approximate eigentrajectories which differ individually to an unknown extent from the desired exact eigentrajectory. To provide some assessment of this discrepancy, we applied the Fourier-based analysis described in Sec. III C to obtain actions for the four sets of correspondence trajectories specified in Table VII. (The transitions whose intensities are determined by these trajectories are given in the footnotes to the table.) Each of the first two sets of correspondence quantum numbers yield, after adiabatic switching, four nonresonant trajectories. The frequencies ω_1, ω_2, and ω_3 in Table VII were estimated from coordinate spectra analogous to those shown in Fig. 5. The action I_1 is seen to be essentially constant over the four trajectories in each case and equal to the desired exact action (given in parentheses). On the other hand, the actions I_2 and I_3 fluctuate considerably about the exact action in each case, approximating it only in an average sense. Each of the second two sets of correspondence quantum numbers in Table VII yield, after adiabatic switching, four 4:1 resonant trajectories. Their frequencies were estimated from coordinate spectra analogous to those shown in Fig. 6, with ω_2 and ω_3 now being interpreted as ω_2^r and ω_3^r; the same interpretation applies to I_2 and I_3. Again the action I_1 is approximately constant for the four trajectories in each case and is very close to the exact action (in parentheses). I_2^r is less than its exact value and fluctuates for $(\frac{1}{2}\,0^0\,\frac{1}{2})$, whereas it is approximately constant and almost equal to the exact value for $(\frac{1}{2}\,0^0\,0)$. For both correspondence states, I_3^r fluctuates considerably and is less than its exact value.

The proximity of the actions of the approximate eigen-

TABLE VII. Fundamental frequencies and actions for several groups of four correspondence trajectories.[a]

$n_1^c(n_2^c)^0 n_3^c$	α_2,α_3[b]	ω_1	ω_2	ω_3	I_1[c]	I_2[c]	I_3[c]
Nonresonant							
01^00[d]	0,0	856.22	524.17	2067.93	0.498	2.037	0.489
	$\pi/2,\pi/2$	857.92	522.99	2067.98	0.498	1.791	0.550
	π,π	856.84	523.64	2067.95	0.498	1.940	0.513
	$3\pi/2,3\pi/2$	855.57	524.41	2067.91	0.499	2.146	0.461
					(0.50)	(2.00)	(0.50)
01.83^00[e]	0,0	849.79	526.69	2063.00	0.499	2.897	0.484
	$\pi/2,\pi/2$	850.82	526.11	2063.00	0.500	2.772	0.515
	π,π	850.93	526.03	2063.00	0.499	2.735	0.524
	$3\pi/2,3\pi/2$	850.21	526.62	2063.00	0.500	2.864	0.492
					(0.50)	(2.83)	(0.50)
Resonant							
$\frac{1}{2}0^0\frac{1}{2}$[f]	0,0	856.71	515.40	4.86	0.996	4.940	0.252
	$\pi/2,\pi/2$	856.25	515.38	5.97	0.999	4.962	0.215
	π,π	855.61	515.33	8.29	0.999	4.983	0.118
	$3\pi/2,3\pi/2$	855.66	515.34	8.00	0.999	4.981	0.134
					(1.00)	(5.00)	(0.50)
$\frac{1}{2}0^00$[g]	0,0	857.90	518.20	6.70	1.000	2.972	0.072
	$\pi/2,\pi/2$	858.52	518.32	4.43	0.994	2.972	0.176
	π,π	858.52	518.32	4.22	0.994	2.971	0.180
	$3\pi/2,3\pi/2$	857.91	518.26	6.53	0.992	2.975	0.075
					(1.00)	(3.00)	(0.50)

[a] Frequencies in cm^{-1} and actions in units of $\hbar = 1$.
[b] Initial values of angle variables for the zeroth-order Hamiltonian; initial value of α_1 is zero for all trajectories.
[c] The desired exact actions for each correspondence state are given in parentheses.
[d] Correspondence quantum numbers for the transition $(0\,0^0\,0) \rightarrow (0\,2^0\,0)$.
[e] Correspondence quantum numbers for the transition $(0\,0^0\,0) \rightarrow (0\,4^0\,0)$.
[f] Correspondence quantum numbers for the transition $(0\,0^0\,0) \rightarrow (1\,0^0\,1)$.
[g] Correspondence quantum numbers for the transition $(0\,0^0\,0) \rightarrow (1\,0^0\,0)$.

trajectories in Table VII to the associated exact actions suggests a hybrid method for the determination of exact eigentrajectories. Namely, the repetitive integration of fairly long trajectories and the search through initial condition space required to obtain eigentrajectories in the Martens and Ezra method[18,31] could probably be minimized by first using the ASM, as described herein, to come "close" to the desired eigentrajectory.

Our last comment concerns a minor modification of the Martens and Ezra analysis for states with $l \neq 0$. Figure 7 displays coordinate spectra for an approximate eigentrajectory with $l = 1$; it is similar to Fig. 5 except for the position of the peak in the q_2 spectrum. This difference arises from the facts that, in our classical treatment, q_2 is a radial coordinate for $l > 0$ and that the fundamental frequency of the radial motion is $2\omega_2$ (see Appendix A for a demonstration of the latter in the zeroth-order description of mode 2). To proceed with the Martens–Ezra analysis, as embodied in Eq. (3.14), one only needs to divide by two the frequency obtained from the q_2 spectrum. Not shown is the associated spectrum of $q_{2x} = q_2 \cos\alpha_l$ (or equivalently $q_{2y} = q_2 \sin\alpha_l$), which is found to have two closely spaced peaks whose average posi-

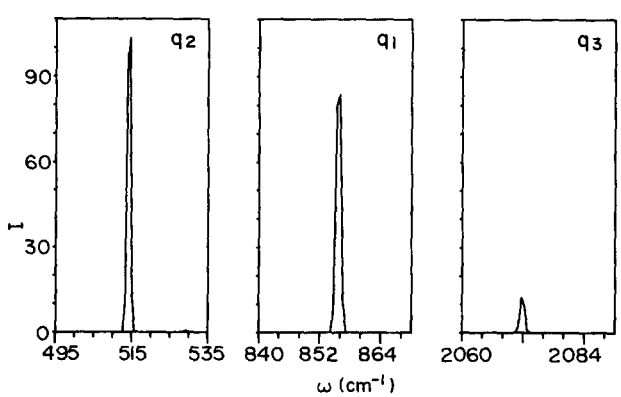

FIG. 5. Typical spectra of the three coordinates q_1, q_2, q_3 in the vicinity of the respective fundamental frequencies for a nonresonant trajectory with $l = 0$. The particular spectra shown were generated by one of the four approximate eigentrajectories for the state $(1\,0^0\,0)$.

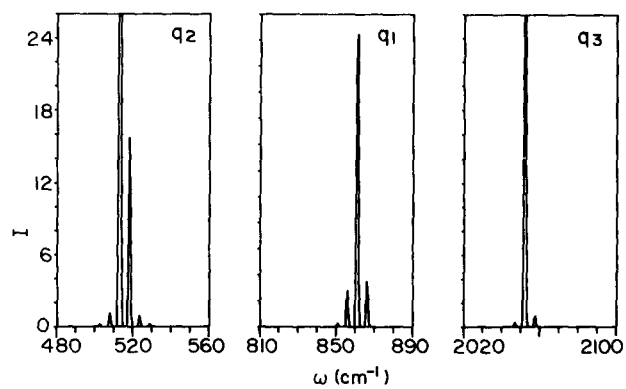

FIG. 6. The same as Fig. 5, but for a resonant trajectory with $l = 0$. Spectra were generated by one of the four approximate eigentrajectories for the state $(0\,0^0\,1)$. The frequency at the center of the largest peak in the q_3 spectrum is four times that of the largest peak in the q_2 spectrum. Note the sidebands in all three spectra.

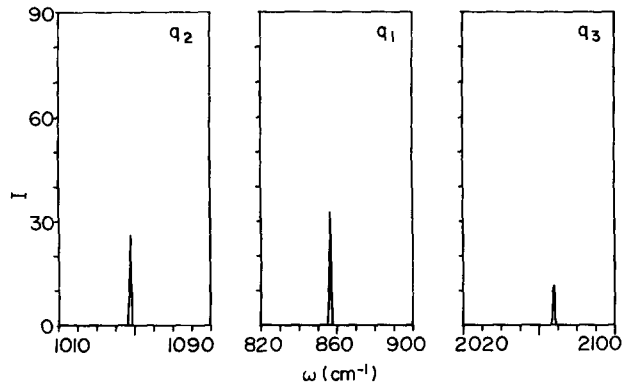

FIG. 7. The same as Fig. 5, but for a nonresonant trajectory with $l = 1$. Spectra were generated by one of the four approximate eigentrajectories for the state $(0\ 1^1\ 0)$. Note that the peak in the q_2 spectrum occurs at twice the frequency of mode 2.

tion is equal to ω_2, within the resolution of the spectra. This splitting is indicative of a fourth independent frequency and is associated with the appearance of α_l, the angle conjugate to $\mathscr{L}$, in the quantity undergoing Fourier transformation. Another perspective on the splitting is the following: if the Hamiltonian were to be perturbed by terms in q_{2x} (or q_{2y}), then the pairwise degeneracy of the $\pm l$ states for a given n_2 would be lifted, the separation of the new nondegenerate states would be given approximately by the splitting in the q_{2x} (or q_{2y}) spectrum, and l would no longer be a good quantum number. Such a splitting occurs for many pairs of zeroth-order states in the Hénon–Heiles system.[4,25]

2. Phase space structure

Each of Figs. 8–10 presents a composite view of the phase space structure of one of the four approximate eigen-

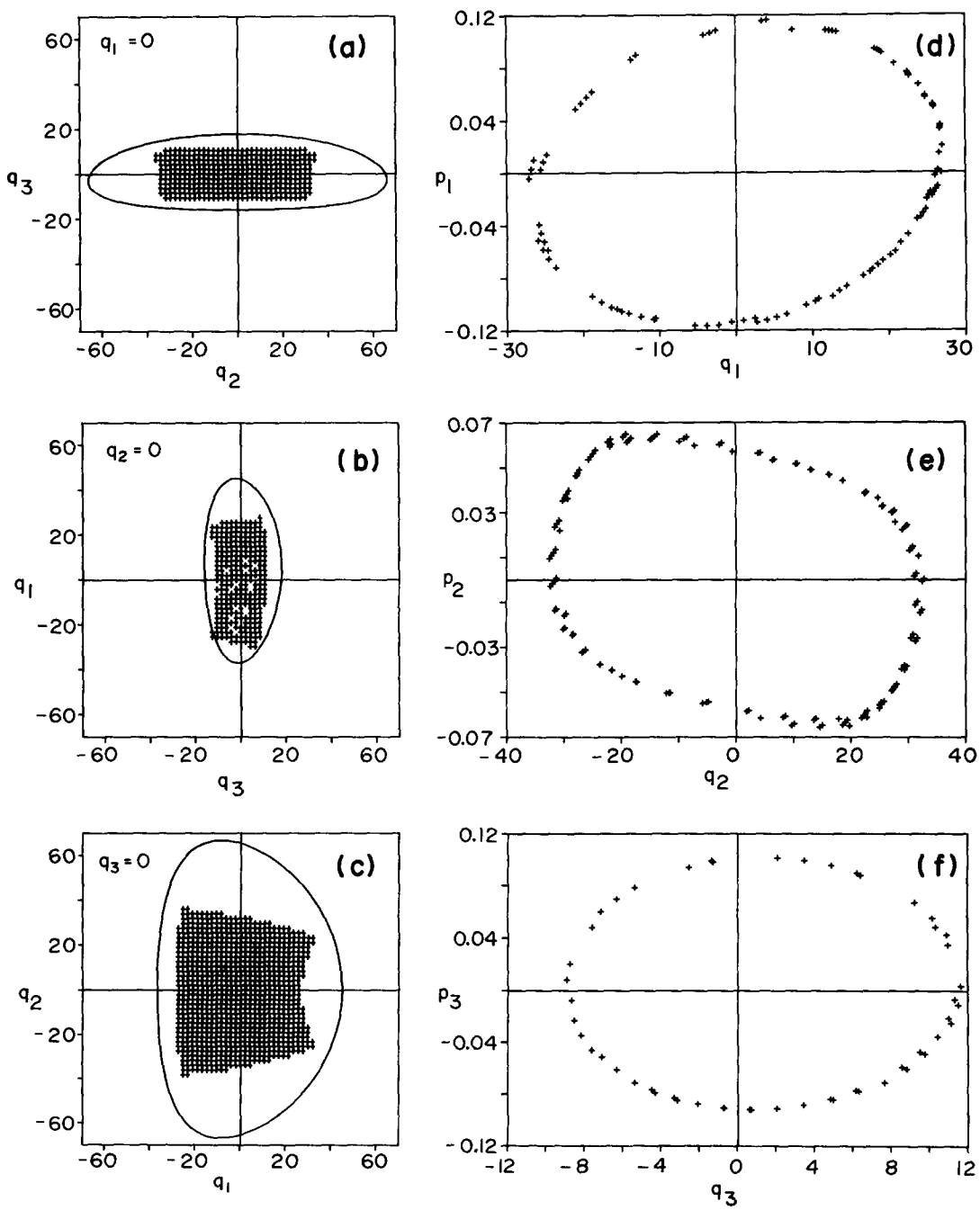

FIG. 8. Phase space structure of the $(1\ 0^0\ 0)$ nonresonant trajectory whose coordinate spectra are displayed in Fig. 5—(a)–(c) configuration space cross sections; (d)–(f) surfaces of section. All coordinates and momenta are in atomic units. The closed curves in (a)–(c) are total energy equipotential contours.

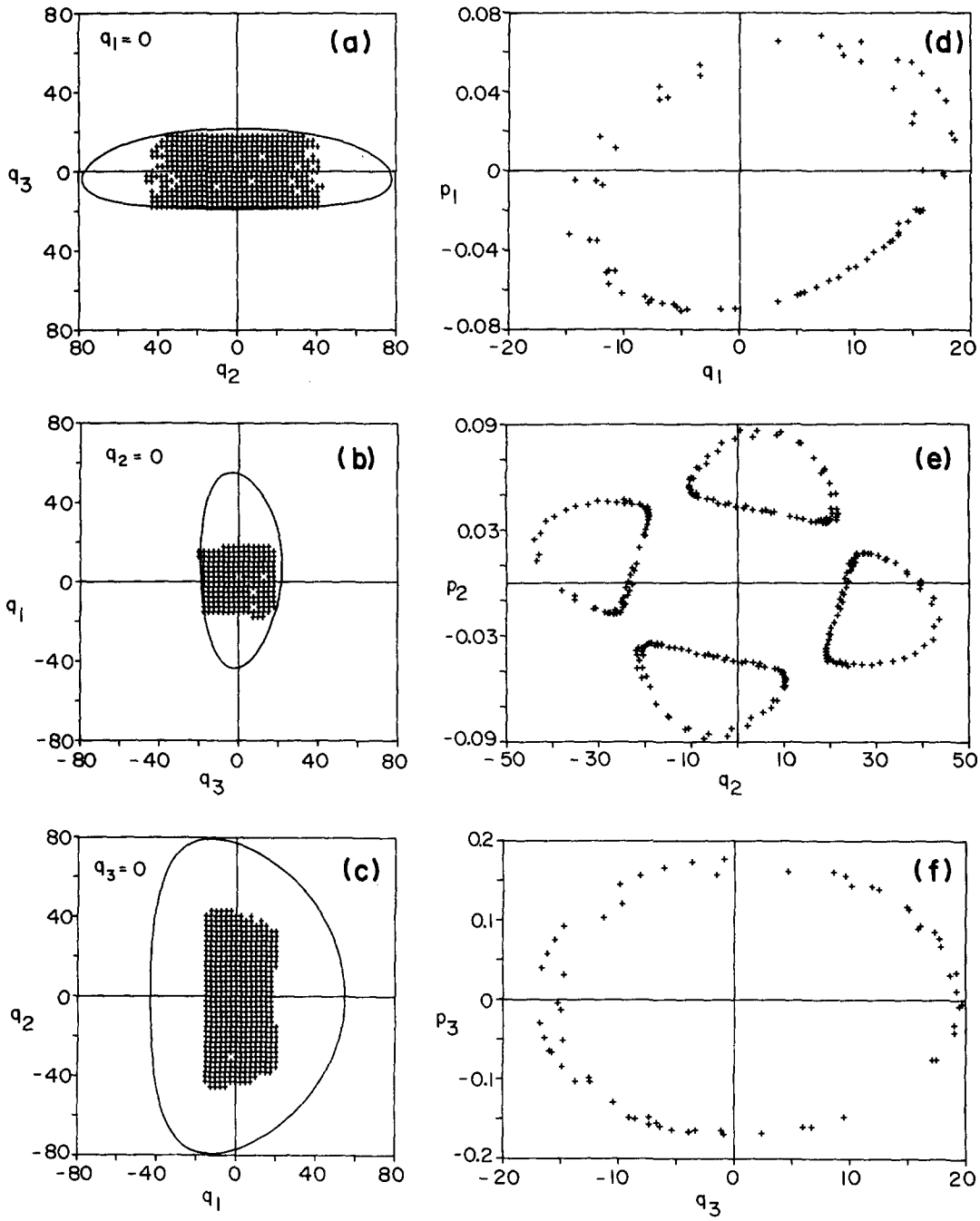

FIG. 9. The same as Fig. 8, but for the (0 0^0 1) resonant trajectory whose coordinate spectra are displayed in Fig. 6.

trajectories obtained via the ASM for a particular OCS vibrational state. Panels (a)–(c) in these figures are configuration space cross sections obtained by holding the third coordinate fixed at the value indicated in each panel. Panels (d)–(f) are p–q surfaces of section; the finite width of the band of points in these plots is attributable to the method used to obtain them. The coordinate spectra in Figs. 5–7 are derived from the same trajectories as Figs. 8–10, respectively.

Figures 8 depicts a nonresonant $l = 0$ trajectory for the state (1 0^0 0) and Fig. 9 is a resonant trajectory with $l = 0$ for the state (0 0^0 1). Comparing these two figures, it is seen that the resonance is evident only in panel (e), the p_2–q_2 surface of section. The cross sections (a)–(c) indicate the differing shapes of the two trajectories but, in this case, offer no evidence of a 4:1 resonance in Fig. 9. However, for several other resonant trajectories studied, the q_3–q_2 cross section did have the "M" shape characteristic of a 4:1 resonance in two dimensions. Figure 10 is an $l = 1$ nonresonant trajectory for the state (0 1^1 0). Here q_2 is a (positive) radial coordinate in the x–y plane, whereas for $l = 0$ (Figs. 8 and 9), it is a 1D Cartesian coordinate. The centrifugal repulsion term in $H_{2,0}$ keeps q_2 away from the origin as is evident in panels (a), (c), and (e). Our phase space views of a precessing type ($l \neq 0$) trajectory are what would be observed in a coordinate system rotating with angular velocity $\dot{\alpha}_l = \partial H / \partial \mathscr{L}$.

VI. SUMMARY

The semiclassical method described in this article is designed to predict vibrational transition frequencies and tran-

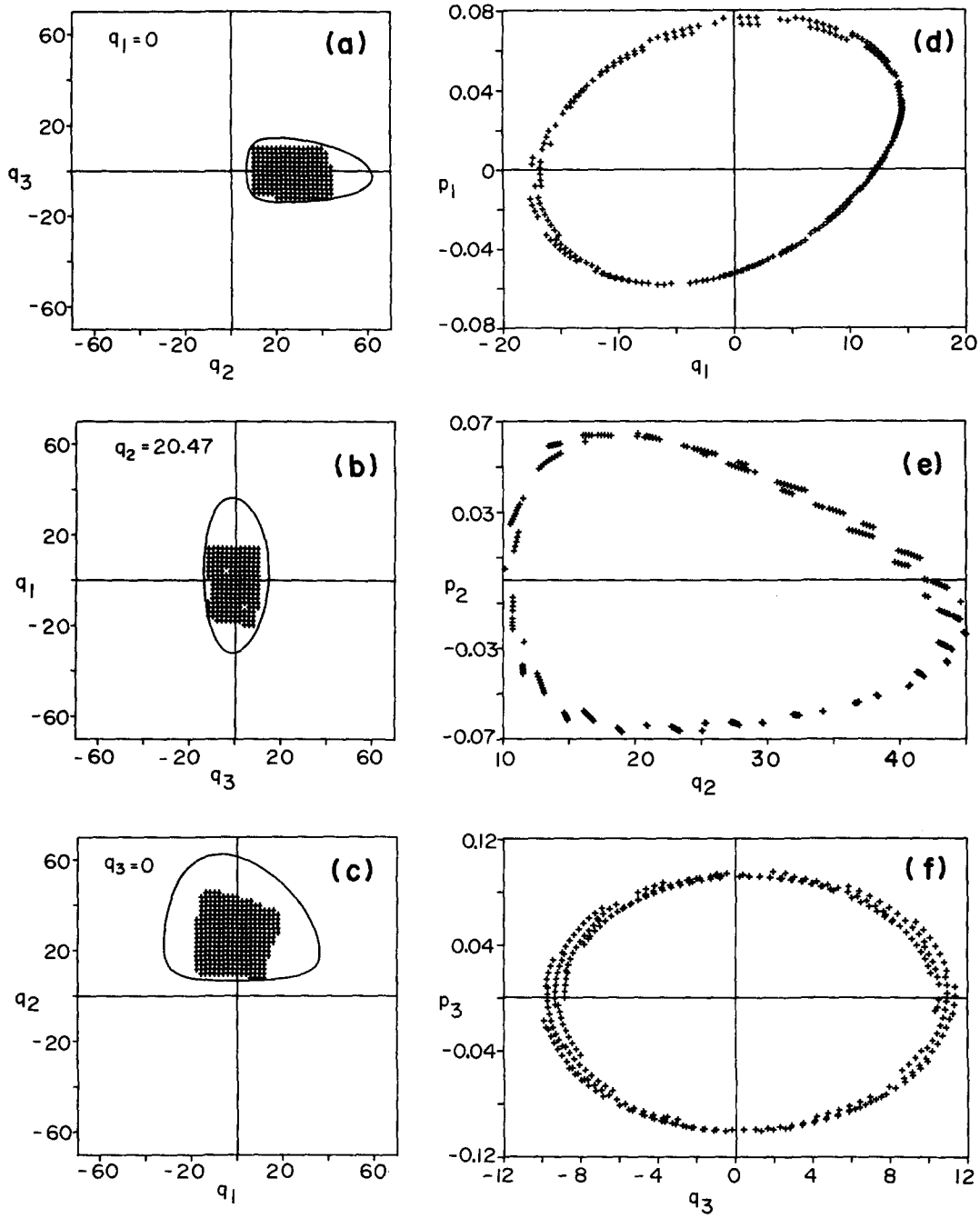

FIG. 10. The same as Fig. 8, but for the $(0\ 1^1\ 0)$ trajectory whose coordinate spectra are displayed in Fig. 7. For $l > 0$, q_2 is the radial coordinate and $0 < q_2 < \infty$, in which case $q_2^{\min}$, rather than $q_2 = 0$, was used to specify the sections in (b), (d), and (f); $q_2^{\min}$ is the position of the minimum in the zeroth order effective potential for mode 2.

sition intensities for small polyatomic molecules. The basic input consists of a potential energy function, a dipole moment function, and a transformation from zeroth-order (uncoupled) action-angle variables to the trajectory integration variables. The method combines (i) the adiabatic switching method for the determination of both eigenvalues and initial conditions of approximate eigentrajectories, and (ii) the power spectral method for the determination of intensities from appropriately selected approximate eigentrajectories. A variety of supplementary techniques are used to assess qualitative and quantitative features of the approximate eigentrajectories.

Our assessment of the utility, validity, and features of the method is based on its application to the vibrational spectroscopy of OCS. A judicious choice of the zeroth-order angle variables, made possible by extension of Johnson's Fourier transform method to three dimensions, reduces to four the size of the ensemble of trajectories required to offset much of the nonadiabaticity arising during the switching process. A switching time of $70\tau_{\text{avg}}$ was found to be optimal, meaning that a total time of $4\times 70\tau_{\text{avg}}$ is required to calculate semiclassical eigenvalues. In terms of computer time, such eigenvalue computations are quite economical and are to be contrasted with quantization schemes involving much longer trajectories, e.g., the surface of section approach[32] or Fourier transform based approaches.[12,18,30] The set of 176 energy levels $E(\text{AS})$ so determined, and expressed as transition frequencies relative to the ground state in Table III, represent the largest available set of semiclassical levels for OCS. Of these, 112 (128) agree with the quantum levels within 1.0 cm^{-1} (2cm^{-1}) and the largest discrepancy is 5.2 cm^{-1}. In all but 11 of the 145 cases, the uncertainty $\Delta E(\text{AS})$

in a semiclassical transition frequency exceeds the difference $|\delta E_1|$ between $E(\mathrm{AS})$ and $E(\mathrm{Q})$, indicating that $\Delta E(\mathrm{AS})$ provides a *reliable* and *built-in* measure of the maximum deviation from $E(\mathrm{Q})$ to be expected. A similar analysis of the 64 available experimental levels reveals that 49 of them agree with $E(\mathrm{AS})$ within 2 cm^{-1} and that $\Delta E(\mathrm{AS})$ provides an upper bound to the difference $|\delta E_2|$ between $E(\mathrm{AS})$ and $E(\mathrm{Q})$ in 41 of 64 cases.

Intensities were determined from the dipole moment power spectrum as generated by a so-called correspondence trajectory. The latter is here an approximate eigentrajectory with zeroth-order actions specified by nonrigorous correspondence rules. The semiclassical results $I(\mathrm{AS})$ are averages of the intensities obtained from the four approximate eigentrajectories generated by the adiabatic switching part of the method. Numerical determination of an intensity to three significant figures is achievable and requires $4\times 1965\tau_{\mathrm{avg}}$, which is about 28 times as long as is required for an energy level computation. If none of the correspondence trajectories contributing to $I(\mathrm{AS})$ is resonant, the semiclassical method is remarkably accurate. In the 17 transitions studied, $I(\mathrm{AS})$ and $I(\mathrm{Q})$ agree within 6%, with 13 of 17 cases agreeing within 3%. In all but three cases, the uncertainty $\Delta I(\mathrm{AS})$ exceeds or is just slightly less than the difference $|\delta I|$ between the semiclassical and quantum results, indicating that it, like $\Delta E(\mathrm{AS})$, usually provides a built-in measure of the maximum expected deviation of $I(\mathrm{AS})$ from $I(\mathrm{Q})$. When any number of the correspondence trajectories contributing to $I(\mathrm{AS})$ is resonant, the (primitive) semiclassical method is comparatively inaccurate. In 8 of the 9 resonant cases studied, $I(\mathrm{AS})$ and $I(\mathrm{Q})$ disagree by more than 6%, the largest difference being 44%. Furthermore, since $\Delta I(\mathrm{AS})$ is no longer found to provide a reliable upper bound to the difference $|\delta I|$, it becomes necessary to identify potentially unreliable $I(\mathrm{AS})$ results by other means. Here, configuration space cross sections, surfaces of section, and spectra of the vibrational coordinates were employed for this purpose. None of these methods require integration of additional trajectories, only additional computer storage space for the relevant data along the *same* trajectory used to generate the power spectrum of the dipole moment function. The occurrence and classification of resonances was most reliably provided by the coordinate spectra, followed by the surfaces of section. The configuration space cross sections proved unreliable in this regard (see Fig. 9). In addition, the coordinate spectra serve two other useful purposes; they can be used (i) to calculate actions thereby providing a quantitative measure of the deviation of the approximate eigentrajectory from the exact eigentrajectory, and (ii) to determine the transition frequency $\boldsymbol{\Delta}\cdot\boldsymbol{\omega}^c$, as would be given by the correspondence trajectory, and hence the location of the relevant peak in the dipole spectrum. A new correspondence rule proposed for mode 2 transitions in which n_2 changes, but $\Delta l = 0$ was found to yield more accurate semiclassical intensity predictions than rules developed for 1D vibrational motion.

ACKNOWLEDGMENTS

Financial support for this research was provided by NSERC of Canada. We thank Professor G. Ezra and Professor T. Uzer for useful discussions concerning certain aspects of the work.

APPENDIX A: CLASSICAL ANALYSIS OF ZEROTH-ORDER DEGENERATE BENDING MOTION

1. Derivation of initial conditions Eq. (3.4) for $l>0$

We first establish that semiclassical quantization of the radial motion with quantized angular momentum action $\mathscr{L} = l\hbar$ recovers the total energy quantization expression $E_{2,0} = (n_2+1)\hbar\omega_{2,0}$. The radial action is

$$\begin{aligned} I_{2r} &= \frac{1}{2\pi}\oint p_{2r}(q_2)\,dq_2 \\ &= \frac{2}{2\pi}\int_{q_{2<}}^{q_{2>}} dq_2\left[2E_{2,0} - \frac{\mathscr{L}^2}{q_2^2} - \omega_{2,0}^2 q_2^2\right]^{1/2} \\ &= \frac{1}{\pi}\int_{q_{2<}}^{q_{2>}} dq_2\,[2E_{2,0}q_2^2 - \mathscr{L}^2 - \omega_{2,0}^2 q_2^4]^{1/2}/q_2. \end{aligned} \tag{A1}$$

The replacement of p_{2r} in the second equality follows from Eq. (2.5). The inner and outer turning points $q_{2<}$, $q_{2>}$ are the positive roots of the quantity in square brackets in Eq. (A1); these roots are real if $E_{2,0} \geqslant \mathscr{L}\omega_{2,0}$, a condition which will be seen to be consistent with the physical requirement that $I_{2r} > 0$. The third integral in Eq. (A1) can be solved[36] by making the substitution $x = q_2^2$, with the following result:

$$I_{2r} = \frac{E_{2,0}}{2\omega_{2,0}} - \frac{\mathscr{L}}{2}. \tag{A2}$$

Imposing the semiclassical quantization condition $I_{2r} = (n_{2r}+\frac{1}{2})\hbar$ yields

$$\begin{aligned} E_{2,0} &= (2I_{2r} + \mathscr{L})\omega_{2,0} \\ &= (2n_{2r} + l + 1)\hbar\omega_{2,0} \\ &= (n_2+1)\hbar\omega_{2,0}, \end{aligned} \tag{A3}$$

which is the desired result.

To determine the radial position q_2 as a function of the angle α_2 conjugate to I_{2r}, it is convenient to begin by establishing the time t associated with q_2 for $q_{2<} \leqslant q_2 \leqslant q_{2>}$:

$$\begin{aligned} t &= \int_{q_{2<}}^{q_2} dq_2/p_{2r} \\ &= \int_{q_{2<}}^{q_2} dq_2\, q_2[2E_{2,0}^2 q_2^2 - \mathscr{L}^2 - \omega_{2,0}^2 q_2^4]^{-1/2} \\ &= \frac{1}{2\omega_{2,0}}\left[\frac{\pi}{2} - \arcsin\left(\frac{E_{2,0} - \omega_{2,0}^2 q_2^2}{\sqrt{E_{2,0}^2 - \mathscr{L}^2\omega_{2,0}^2}}\right)\right]. \end{aligned} \tag{A4}$$

The period of the radial motion is obtained by evaluating Eq. (A4) at $q_{2>}$ and found to be $\tau_{2r} = \pi/\omega_{2,0}$, which is the period of an oscillator with frequency $2\omega_{2,0}$. Since $\alpha_2(t) = 2\omega_{2,0}(t)$, we have from Eq. (A4),

$$\sin\left(\alpha_2 - \frac{\pi}{2}\right) = -\frac{E_{2,0} - \omega_{2,0}^2 q_2^2}{\sqrt{E_{2,0}^2 - \mathscr{L}^2\omega_{2,0}^2}},$$

which when solved for q_2 with the restriction $0 \leqslant \alpha_2 \leqslant \pi$ yields Eq. (3.6a),

$$q_2 = \frac{1}{\omega_{2,0}}\left[(E_{2,0}^2 - \mathscr{L}^2\omega_{2,0}^2)^{1/2} \times \sin\left(\alpha_2 - \frac{\pi}{2}\right) + E_{2,0}\right]^{1/2}. \quad \text{(A5)}$$

Equation (3.6b) is obtained by substituting for q_2 in the zeroth-order Hamiltonian $H_{2,0}$ [Eq. (2.5)] and solving for p_{2r}.

2. Derivation of correspondence rule (3.12) for $\Delta l = 0$ transitions

To arrive at a correspondence rule, we follow Naccache[1] who compares, for 1D harmonic and Morse oscillators, quantum matrix elements of powers of the coordinates and momenta to the associated classical Fourier coefficients. The dipole μ_z [Eq. (2.10)], which induces the $\Delta l = 0$ transitions here, has a mode 2 coordinate dependence of Q_2^2, so that the zeroth-order selction rule is $\Delta n_2 = 2$. Since the eigenfunctions of the full Hamiltonian H are linear combinations of the basis states, the general selection rule becomes Δn_2 = even. However, transitions with $\Delta n_2 > 4$ are found to have sufficiently small intensities that only $\Delta n_2 = 2,4$ transitions are reported in our study. In what follows, we therefore only consider matrix elements and Fourier coefficients of the dimensionless quantities Q_2^2 and Q_2^4.

The Fourier representation of Q_2^2 for given quantum numbers (n_2,l) follows immediately from Eq. (A5),

$$\begin{aligned} Q_2^2 &= \frac{\omega_{2,0}q_2^2}{\hbar} \\ &= \frac{1}{\hbar\omega_{2,0}}\left[E_{2,0} - (E_{2,0}^2 - \mathscr{L}^2\omega_{2,0}^2)^{1/2}\cos(2\omega_{2,0}t)\right] \\ &= (n_2+1) - \sqrt{(n_2+1)^2 - l^2}\cos(2\omega_{2,0}t) \\ &= (n_2+1) - \sqrt{(n_2+1)^2 - l^2}\tfrac{1}{2}\{e^{i2\omega_{2,0}t} + e^{-2\omega_{2,0}t}\}. \end{aligned} \quad \text{(A6)}$$

Squaring Eq. (A6) yields the Fourier representation of Q_2^4:

$$\begin{aligned} Q_2^4 = {} & \tfrac{1}{4}[(n_2+1)^2 - l^2]\{e^{i4\omega_{2,0}t} + e^{-i4\omega_{2,0}t}\} \\ & - (n_2+1)\sqrt{(n_2+1)^2 - l^2}\{e^{i2\omega_{2,0}t} + e^{-i2\omega_{2,0}t}\} \\ & + \tfrac{3}{2}[n_2^2 + 6n_2 - l^2 + \tfrac{4}{3}]. \end{aligned} \quad \text{(A7)}$$

TABLE IX. Convergence of semiclassical intensity results for transitions from the ground state.[a]

Final state	$\omega(1/2)$[b]	ω[c]	$\omega(2)$[d]	$I(1/2)$[b,e]	I[c,e]	$I(2)$[d,e]
10^00	f	857.9	857.8	f	3.42(3)	3.42(3)
02^00	1048.4	1048.2	1048.1	8.89(3)	8.89(3)	8.89(3)
20^00	1712.5	1712.2	1712.1	5.78(4)	5.78(4)	5.78(4)
01^10	519.9	520.1	520.0	1.43(3)	1.10(3)	1.10(3)

[a] Frequencies in cm^{-1} and intensities in $(Debye)^2$; for a given transition all entries were determined from the dipole spectrum of one of the four correspondence trajectories involved in the present semiclassical treatment.
[b] Trajectory integrated for $982.5\tau_{avg}$.
[c] Trajectory integrated for $1965\tau_{avg}$; the majority of the I(AS) results in Table IV were obtained from trajectories of this length.
[d] Trajectory integrated for $3930\tau_{avg}$.
[e] Number in parentheses is the negative of the power of 10.
[f] Data not available.

Table VIII lists all nonzero matrix elements of Q_2^2 and Q_2^4 in the polar basis set used for mode 2. Comparison of the quantum mechanical value of each matrix element to the appropriate Fourier coefficient in Eqs. (A6) and (A7) leads to the correspondence values in the last column. The associated correspondence quantum number n_2^c is given by

$$n_2^c = \begin{cases} 2\left[\left\{\dfrac{n_2^i + \Delta_2}{2}\right\}!/(n_2^i/2)!\right]^{2/\Delta_2} - 1, & \text{if } \Delta_2 > 0 \\ n_2^i, & \text{if } \Delta_2 = 0 \end{cases} \quad \text{(A8)}$$

where $\Delta_2 = n_2^f - n_2^i$ is always chosen to be positive. The semiclassical results in Table VIII are exact for all but the two $\Delta_2 = 4$ matrix elements. In these two cases, the indicated correspondence is exact only for $l = 0$, but can be shown to provide an excellent approximation to the quantum result by comparing these two quantities for, say, the $n_2 \to n_2 + 4$ transition. Using Eq. (A8) for n_2^c, the correspondence result can be written as $\frac{1}{4}[(n_2+2)^2(n_2+4)^2 + l^4 - 2l^2(n_2+2)(n_2+4)]^{1/2}$, whereas the quantum result from Table VIII is $\frac{1}{4}[(n_2+2)^2(n_2+4)^2 + l^4 - 2l^2[(n_2+2)^2 + (n_2+4)^2]/2]^{1/2}$. These differ only in that the average of the squares of (n_2+2) and (n_2+4) in the quantum expression is replaced by their product in the correspondence

TABLE VIII. Comparison of quantum mechanical and correspondence values for matrix elements of $Q_2^{2\lambda}$ for $\lambda = 1,2$.

$\langle n_2^i \lvert Q_2^{2\lambda} \rvert n_2^i + \Delta_2\rangle$	Quantum value	Correspondence value[a]
$\langle n_2 \lvert Q_2^2 \rvert n_2+2\rangle$	$-\frac{1}{2}[(n_2+2)^2 - l^2]^{1/2}$	$-\frac{1}{2}[(n_2^c+1)^2 - l^2]^{1/2}$
$\langle n_2-2 \lvert Q_2^2 \rvert n_2\rangle$	$-\frac{1}{2}[n_2^2 - l^2]^{1/2}$	$-\frac{1}{2}[(n_2^c+1)^2 - l^2]^{1/2}$
$\langle n_2 \lvert Q_2^2 \rvert n_2\rangle$	$n_2 + 1$	$n_2^c + 1$
$\langle n_2 \lvert Q_2^4 \rvert n_2+4\rangle$[b]	$\frac{1}{4}\{[(n_2+2)^2 - l^2][(n_2+4)^2 - l^2]\}^{1/2}$	$\frac{1}{4}[(n_2^c+1)^2 - l^2]$
$\langle n_2-4 \lvert Q_2^4 \rvert n_2\rangle$[b]	$\frac{1}{4}[(n_2^2 - l^2)(n_2^2 - l^2)]^{1/2}$	$\frac{1}{4}[(n_2^c+1)^2 - l^2]$
$\langle n_2 \lvert Q_2^4 \rvert n_2+2\rangle$	$-(n_2+2)[(n_2+2)^2 - l^2]^{1/2}$	$-(n_2^c+1)[(n_2^c+1)^2 - l^2]^{1/2}$
$\langle n_2-2 \lvert Q_2^4 \rvert n_2\rangle$	$-n_2[n_2^2 - l^2]^{1/2}$	$-(n_2^c+1)[(n_2^c+1)^2 - l^2]^{1/2}$
$\langle n_2 \lvert Q_2^4 \rvert n_2\rangle$	$\frac{3}{2}[n_2^2 + 6n_2 + \frac{4}{3} - l^2]$	$\frac{3}{2}[(n_2^c)^2 + 6n_2^c + \frac{4}{3} - l^2]$

[a] Expressions for n_2^c are given in Appendix A.
[b] Approximate correspondence result; justification is discussed in Appendix A.

expression. Since $[(n_2+2)^2+(n_2+4)^2]/2-(n_2+2)(n_2+4)=2$ for all n_2, the aforementioned replacement is a good approximation.

APPENDIX B: FOURIER ANALYSIS OF $E(\mathbf{I},\boldsymbol{\alpha},T)$

1. Theory

This analysis relies on the observation that the initial conditions are periodic in $\boldsymbol{\alpha}$, and therefore E is also a periodic function of $\boldsymbol{\alpha}$. The energy is represented by a Fourier series

$$E(\mathbf{I},\boldsymbol{\alpha},T)=A_{000}+\sum_{\mathbf{k}}{}'A_{\mathbf{k}}(\mathbf{I},T)e^{i\mathbf{k}\cdot\boldsymbol{\alpha}}, \tag{B1}$$

where the elements of $\mathbf{k}$ range over positive and negative integers, excluding zero, and A_{000} is the average of $E(\mathbf{I},\boldsymbol{\alpha},T)$ over $\boldsymbol{\alpha}$. The Fourier coefficients $A_{\mathbf{k}}$ can be evaluated for a uniform grid of α's. If the summations are truncated to $2L_i+1$ terms, Eq. (B1) can be rewritten as

$$E_{j_1j_2j_3}\cong\sum_{k_1=-L_1}^{L_1}\sum_{k_2=-L_2}^{L_2}\sum_{k_3=-L_3}^{L_3}A_{k_1k_2k_3}\times\exp\{i(\alpha_{j_1}k_1+\alpha_{j_2}k_2+\alpha_{j_3}k_3)\}, \tag{B2}$$

where $\alpha_{j_i}=2\pi j_i/N_i$ is an angle on an evenly spaced grid specified by $j_i=0,1,\ldots,N_i-1$ for mode $i=(i=1,2,3)$. The coefficients $A_{k_1k_2k_3}$ are evaluated from the discrete Fourier transform of $E_{j_1j_2j_3}$; this is a generalization to three dimensions of Johnson's derivation.[8] For given actions $\mathbf{I}=(I_1,I_2,I_3)$, switching time T, and multidimensional grid of angles, the final energy $E_{j_1j_2j_3}=E(\alpha_{j_1},\alpha_{j_2},\alpha_{j_3})$ is computed. The discrete Fourier transform is evaluated

$$F_{\mu\nu\sigma}=\frac{1}{N_1N_2N_3}\sum_{j_1=0}^{N_1-1}\sum_{j_2=0}^{N_2-1}\sum_{j_3=0}^{N_3-1}E_{j_1j_2j_3}\times\exp\left\{-2\pi i\left[\frac{j_1\mu}{N_1}+\frac{j_2\nu}{N_2}+\frac{j_3\sigma}{N_3}\right]\right\}, \tag{B3}$$

where $0\leqslant\mu\leqslant N_1-1$, $0\leqslant\nu\leqslant N_2-1$, $0\leqslant\sigma\leqslant N_3-1$, and $N_i=2L_i+1$.

The Fourier series can be rewritten as

$$E_{j_1j_2j_3}=A_{000}+\sum_{k_1k_2k_3}{}'A_{k_1k_2k_3}\times\exp\left\{2\pi i\left[\frac{j_1k_1}{N_1}+\frac{j_2k_2}{N_2}+\frac{j_3k_3}{N_3}\right]\right\}, \tag{B4}$$

where the prime indicates that the $\mathbf{k}=0$ term is omitted. Substituting Eq. (B4) into Eq. (B3) yields

$$\begin{aligned}F_{\mu\nu\sigma}&=\frac{1}{N_1N_2N_3}\sum_{j_1=0}^{N_1-1}\sum_{j_2=0}^{N_2-1}\sum_{j_3=0}^{N_3-1}\left\{A_{000}+\sum_{k_1k_2k_3}{}'A_{k_1k_2k_3}\right.\\&\quad\times\exp\left[2\pi i\left(\frac{(k_1-\mu)j_1}{N_1}+\frac{(k_2-\nu)j_2}{N_2}\right.\right.\\&\quad\left.\left.\left.+\frac{(k_3-\sigma)j_3}{N_3}\right)\right]\right\}\\&=A_{000}+\sum_{k_1k_2k_3}{}'A_{k_1k_2k_3}\delta_{k_1\pm n_1N_1,\mu}\delta_{k_2\pm n_2N_2,\nu}\delta_{k_3\pm n_3N_3,\sigma},\end{aligned} \tag{B5}$$

where $n_i=0,1,\ldots$. The relationship between $A_{k_1k_2k_3}$ and the Fourier transform follows:

$$A_{\mathbf{k}}=F_{\mathbf{m}},$$

where

$$m_i=\begin{cases}k_i & \text{for } k_i=0,\ldots,L_i\\ 2L_i+1+k_i & \text{for } k_i=-1,\ldots,-L_i\end{cases}. \tag{B6}$$

2. Application to OCS

For selected actions $\mathbf{I}$ corresponding to vibrational states of OCS, values of $E_{j_1j_2j_3}$ were determined by adiabatic switching on various grids of angles as specified by (N_1,N_2,N_3). The coefficients $A_{k_1k_2k_3}$ in Eq. (B1) were determined via Eqs. (B3)–(B6). It was found that the first mode had little influence on the energy, since the dominant coefficients are of the form A_{0mn}. The four dominant coefficients are A_{02-1}, A_{011} and their complex conjugates. [Since $E(\mathbf{I},T)$ is real, complex conjugate coefficients are associated with $-\mathbf{k}$ terms in Eq. (B1).] A useful approximate expansion for the energy is therefore obtained by setting $\alpha_1=0$ and retaining only the dominant coefficients in the Fourier expansion

$$\begin{aligned}E(\mathbf{I},\boldsymbol{\alpha},T)\cong&A_{000}+A_{02-1}\exp\{2i\alpha_2-i\alpha_3\}+A^*_{02-1}\\&\times\exp\{-(2i\alpha_2-i\alpha_3)\}\\&+A_{011}\exp\{i\alpha_2+i\alpha_3\}\\&+A^*_{011}\exp\{-(i\alpha_2+i\alpha_3)\}.\end{aligned} \tag{B7}$$

The desired semiclassical eigenvalue is then approximated as the average energy of a group of four trajectories chosen to eliminate the dominant Fourier coefficients

$$\begin{aligned}E[\mathbf{I},(0,0,0),T]&\cong\bar{E}(\mathbf{I},T)+A_{02-1}+A^*_{02-1}\\&\quad+A_{011}+A^*_{011},\\E[\mathbf{I},(0,\pi/2,\pi/2),T]&\cong\bar{E}(\mathbf{I},T)+iA_{02-1}-iA^*_{02-1}\\&\quad-A_{011}-A^*_{011},\\E[\mathbf{I},(0,\pi,\pi),T]&\cong\bar{E}(\mathbf{I},T)-A_{02-1}-A^*_{02-1}\\&\quad+A_{011}+A^*_{011},\\E[\mathbf{I},(0,3\pi/2,3\pi/2),T]&\cong\bar{E}(\mathbf{I},T)-iA_{02-1}+iA^*_{02-1}\\&\quad-A_{011}-A^*_{011},\end{aligned} \tag{B8}$$

where the equivalence of A_{000} and the mean energy $\bar{E}(\mathbf{I},T)$ has been made explicit.

APPENDIX C: NUMERICAL DETERMINATION OF SEMICLASSICAL INTENSITIES

Intensities were extracted from trajectories via Fourier transformation of the time dependence of the dipole moment function on a finite time interval. Details of this procedure are given in the Appendix of Ref. 4, apart from the improvement described immediately below.

When calculating the power spectra of data sampled over a finite interval, one is effectively multiplying an infinite periodic extension of the data by a square window, which is 0 outside and 1 inside the interval. This results in a spectrum with widened peaks and spurious sidebands. To remedy this situation, one multiplies the data with a window which changes more gradually from 0 to its maximum. We used the

— 74 dB Blackmann–Harris window function.[37] To correct for the scaling effect of a window, one divides the spectrum of the windowed data by the mean-squared amplitude of the window, i.e., by $(1/N)\sum_{n=0}^{N-1} W(n)^2$, where N is the number of discrete points comprising the spectrum and

$$W(n) = \sum_{j=0}^{3} (-1)^j a_j \cos\left(\frac{2\pi jn}{N}\right), \quad n = 0,1,2,\ldots,N-1$$

with $a_0 = 0.402\,17$, $a_1 = 0.497\,03$, $a_2 = 0.093\,92$, $a_3 = 0.001\,83$.

Spectra were calculated using a fast Fourier transform (FFT) routine and the intensity obtained as the area under the peak corresponding to the frequency of the transition in question. Technical details of the FFT as applied to OCS are as follows: A time step of $\delta = 0.120\tau_{avg}$ was used, in order to ensure a sufficiently large frequency range in the spectrum: $\omega_{max} = \pi/\delta = 4850\ \text{cm}^{-1}$. These trajectories were continued long enough to achieve convergence of the spectral intensities to three significant figures, as is illustrated in Table IX for a few selected trajectories. For all but a few intensities, the required time is $1965\tau_{avg}$, which corresponds to 2^{14} discrete time steps δ and to a spectral resolution of $2\pi/1965\tau_{avg} \approx 0.6\ \text{cm}^{-1}$; several cases required $3930\tau_{avg}$ to achieve convergence of the intensity.

Hamilton's equations of motion were solved using Shampine and Gordon's ODE integrator.[38] Selected trajectories were back integrated to at least two significant figures in the momenta and six figures in the coordinates.

[1]P. F. Naccache, J. Phys. B. **5**, 1308 (1972).
[2]M. L. Koszykowski, D. W. Noid, and R. A. Marcus, J. Phys. Chem. **86**, 2113 (1982).
[3]J. R. Stine and D. W. Noid, J. Chem. Phys. **78**, 1876 (1983).
[4]D. M. Wardlaw, D. W. Noid, and R. A. Marcus, J. Phys. Chem. **88**, 536 (1984).
[5]S. M. Colwell, N. C. Handy, and W. H. Miller, J. Chem. Phys. **68**, 745 (1978); P. Pajunen, *ibid.* **83**, 2363 (1985); J. H. Frederick and G. M. McLelland, *ibid.* **84**, 876 (1986); R. J. Duchovic and G. C. Schatz, *ibid.* **84**, 2239 (1986).
[6]J. E. Adams, J. Chem. Phys. **84**, 3589 (1986).
[7]R. T. Skodje, F. Borondo, and W. P. Reinhardt, J. Chem. Phys. **82**, 4611 (1985).
[8]B. R. Johnson, J. Chem. Phys. **83**, 1204 (1985).
[9]I. C. Percival and N. Pomphrey, Mol. Phys. **35**, 649 (1978).
[10]S. M. Colwell, Chem. Phys. **46**, 165 (1980).
[11]N. C. Handy, S. M. Colwell, and W. H. Miller, Faraday Discuss. Chem. Soc. **62**, 29 (1977); S. M. Colwell and N. C. Handy, Mol. Phys. **35**, 1183 (1978); G. C. Schatz and T. Mulloney, J. Chem. Phys. **83**, 989 (1979).
[12]C. W. Eaker and G. C. Schatz, J. Chem. Phys. **81**, 2394 (1984).
[13]B. R. Johnson, J. Chem. Phys. **86**, 1445 (1987).
[14]A. Foord, J. G. Smith, and D. H. Whiffen, Mol. Phys. **29**, 1685 (1975).
[15]K. Tanaka, T. Tanaka, and I. Suzuki, J. Chem. Phys. **82**, 2835 (1985).
[16]A. Fayt, Ann. Soc. Sci. Brux. **86**, 61 (1972).
[17]D. Carter and P. Brumer, J. Chem. Phys. **77**, 4208 (1982); M. J. Davis, Chem. Phys. Lett. **110**, 491 (1984).
[18]C. E. Martens and G. S. Ezra, J. Chem. Phys. **83**, 2990 (1985).
[19]C. Jaffe and P. Brumer, J. Phys. Chem. **88**, 4829 (1984); J. Chem. Phys. **82**, 2330 (1985).
[20]R. B. Shirts, J. Phys. Chem. **91**, 2258 (1987).
[21]J. K. G. Watson, Mol. Phys. **19**, 465 (1970).
[22]J. T. Hougen, J. Chem. Phys. **36**, 519 (1962).
[23]R. T. Skodje and F. Borondo, Chem. Phys. Lett. **118**, 409 (1985); J. Chem. Phys. **84**, 1533 (1986); T. P. Grozdanov, S. Saini, and H. S. Taylor, *ibid.* **84**, 3243 (1986).
[24]The 2D rotational motion is degenerate with respect to the sign of l. Since the Hamiltonian given by Eq. (2.1) does not lift this degeneracy, it suffices to consider only positive values of l.
[25]D. W. Noid and R. A. Marcus, J. Chem. Phys. **67**, 559 (1977).
[26]P. Ehrenfest, Verslagen Kon. Akad. Amsterdam **25**, 412 (1916). An abridged English translation appears in *Sources of Quantum Mechanics*, edited by B. L. Van Der Waerden (Dover, New York, 1967); E. A. Solov'ev, Sov. Phys. **48**, 635 (1978).
[27]D. W. Noid, M. L. Koszykowski, and R. A. Marcus, J. Chem. Phys. **67**, 404 (1977).
[28]A degenerate system requires an ensemble of trajectories, chosen so as to average over the phases corresponding to the zero frequency modes.
[29]N. Bohr, in *On the Quantum Theory of Line Spectra* in *Sources of Quantum Mechanics*, edited by B. L. Van der Waerden (Dover, New York, 1967), pp. 95–137; J. H. Van Vleck, Bull. Natl. Res. Council U.S.A. **10**, 1 (1926), Part 4; J. H. Van Vleck, Phys. Rev. **24**, 330 (1924); E. C. Kemble, *ibid.* **25**, 1 (1925); Proc. Natl. Acad. Sci. U.S.A. **10**, 274 (1924); R. H. Fowler, Philos. Mag. **49**, 1272 (1925); F. C. Hoyt, *ibid.* **46**, 135 (1923); **47**, 826 (1924).
[30]I. C. Percival and D. J. Richards, J. Phys. B. **3**, 1035 (1970).
[31]C. E. Martens and G. S. Ezra, J. Chem. Phys. **86**, 279 (1987).
[32]D. W. Noid, D. M. Wardlaw, M. L. Koszykowski, and R. A. Marcus, J. Phys. Chem. **87**, 2733 (1983).
[33]D. W. Noid, M. L. Koszykowski, and R. A. Marcus, J. Chem. Phys. **73**, 391 (1980).
[34]J. D. Louck and W. H. Shaffer, J. Mol. Spectrosc. **4**, 285 (1960).
[35]*Handbook of Mathematical Functions*, edited by M. Abramowitz and I. A. Stegun (Dover, New York, 1972)
[36]I. S. Gradshteyn and I. M. Ryzhik, *Tables of Integrals, Series, and Products* (Academic, New York, 1965).
[37]F. J. Harris, Proc. IEEE **66**, 51 (1978).
[38]M. K. Gordon, Sandia Laboratories Report, SAND 75-0211. For a discussion of the algorithm see L. F. Shampine and M. K. Gordon, *Computer Solution of Ordinary Differential Equations* (Freeman, San Francisco, 1975).
[39]M. L. Koszykowski, G. A. Pfeffer, and D. W. Noid, Ann. N.Y. Acad. Sci. **497**, 127 (1987).